ELSEVIER

Chemical Engineering Science 59 (2004) 2567–2592

Chemical Engineering Science

www.elsevier.com/locate/ces

Numerical solution of the spatially distributed population balance equation describing the hydrodynamics of interacting liquid–liquid dispersions

Menwer M. Attarakih[a], Hans-Jörg Bart[a,*], Naim M. Faqir[b]

[a] *Faculty of Mechanical & Process Engineering, The University of Kaiserslautern, Institute of Thermal Process Engineering, POB 3049, D-67653 Kaiserslautern, Germany*

[b] *Chemical Engineering Department, Faculty of Engineering & Technology, The University of Jordan, 11942 Amman, Jordan*

Received 14 October 2003; received in revised form 2 March 2004; accepted 5 March 2004

Abstract

In liquid–liquid contacting equipment such as completely mixed and differential contactors, droplet population balance based modeling is now being used to describe the complex hydrodynamic behavior of the dispersed phase. For the hydrodynamics of these interacting dispersions this model accounts for droplet breakage, droplet coalescence, axial dispersion, exit and entry events. The resulting population balance equations are integro-partial differential equations (IPDE) that rarely have an analytical solution, especially when they show spatial dependency, and hence numerical solutions are sought in general. To do this, these IPDEs are projected onto a system of convective dominant partial differential equations by discretizing the droplet diameter (internal coordinate). This is accomplished by generalizing the fixed-pivot (GFP) technique of Kumar and Ramkrishna (Chem. Eng. Sci. 51 (1996a) 1311) handling any two integral properties of the population number density for continuous flow systems by treating the inlet feed distribution as a source term. Moreover, the GFD technique has the advantage of being free of repeated or double integral evaluation resulting from the weighted residual approaches such as the Galerkin's method. This allows the time-dependent breakage and coalescence functions to be easily handled without appreciable increase in the computational time. The resulting system of PDEs is spatially discretized in conservative form using a simplified first order upwind scheme as well as first- and second-order non-oscillatory central differencing schemes. This spatial discretization avoids the characteristic decomposition of the convective flux based on the approximate Riemann solvers and the operator splitting technique required by classical upwind schemes. The time variable is discretized using an implicit strongly stable approach that is formulated by careful lagging of the non-linear parts of the convective and source terms. The algorithm is tested against analytical solutions of the simplified population balance equation for a differential liquid–liquid extraction column through four case studies. In all these case studies the discrete models converge successfully to the available analytical solutions and to solutions on relatively fine grids when the analytical solution is not available. Realization of the algorithm is accomplished by comparing its predictions to experimental steady-state hydrodynamic data of a laboratory scale rotating disc contactor of 0.15 m diameter. Practically, the combined algorithm is found fast enough for the computation of the transient and steady-state hydrodynamic behavior of the continuously and spatially distributed interacting liquid–liquid dispersions.

Keywords: Liquid–liquid dispersion; Population balance; Droplet breakage; Droplet coalescence; Conservation laws; Numerical simulation

1. Introduction

The modeling of the multi-phase flow systems occurring in chemical engineering is now widely accepted based on the population balance concept. Within this framework it appears that Hulburt and Katz (1964) and Valentas and Amundson (1966) were among the first who introduced the population balance equation (PBE) into the modeling of chemical engineering processes involving dispersed phase operations. Such processes include unit operations carried out in batch and continuous stirred tanks as well as in differential contacting equipment such as crystallization (Motz et al., 2002), bubble (Campos and Lage, 2003) and liquid–liquid extraction columns (LLEC) (Modes et al., 1999; Gerstlauer, 1999). In such unit operation equipment the dynamically changing behavior of the dispersed particles,

* Corresponding author. Tel.: +49-631-205-2414; fax: +49631205119.
E-mail address: bart@mv.uni-kl.de (H.-J. Bart).
URL: http://www.uni-kl.de/LS-Bart/

0009-2509/$ - see front matter © 2004 Elsevier Ltd. All rights reserved.
doi:10.1016/j.ces.2004.03.005

or strictly speaking droplets (or bubbles), makes it necessary to consider a detailed mathematical rather than lumped modeling approach. These details are necessary to describe the discontinuous events occurring due to the interaction of the turbulent continuous and the dispersed phases constituents (droplets) such as breakage and coalescence. Loosely speaking, the term breakage considers the interaction of a single droplet with the turbulent continuous phase where the droplet undergoes breakage if the turbulent kinetic energy transmitted to the droplet exceeds its surface energy (Coulaloglou and Tavlarides, 1977). On the other hand, droplet coalescence is expected to occur due to the interaction between two droplets and the turbulent continuous phase. The coalescence between these two droplets is considered to occur if the intervening liquid film has sufficient contact time to be drained out (Chatzi and Lee, 1987). Consequently, it is expected to find a droplet size distribution along the spatial coordinate of the liquid–liquid contacting equipment making the models inherently assuming uniform droplet size distribution or based on some mean droplet diameter (d32) of little practical value (Alatiqi et al., 1995; Weinstein et al., 1998). Accordingly, the promising modeling of these phenomena, based on the population balances, offers not only the dispersed phase hold-up (volume concentration) but also any integral property associated with the resulting particle (droplet) distribution such as the mean droplet size and the specific interfacial area required for the calculation of mass and heat fluxes (Al Khani et al., 1988; Tsouris et al., 1994; Alopaeus et al., 2002).

The population balance approach could be applied for modeling the behavior of the interacting liquid–liquid dispersions in either two basic ways, namely; the stagewise and the differential models. In the stagewise models (Tsouris et al., 1994; Kentish et al., 1998; Steiner et al., 1999) the multistage column is represented by a sequence of interacting stirred tanks with forward and backward flow components to compensate for the nonideal behavior of each tank. In this sense a population balance equation has to be written for each tank with the required boundary conditions. In the differential model approach (Casamatta and Vogelpohl, 1985; Al Khani et al., 1988, 1989; Cabassud et al., 1990; Modes et al., 1999), the PBE is usually formulated as a conservation law in terms of volume concentration (mass for constant dispersed phase density). The resulting differential model takes into account the droplet transport; breakage and coalescence as well as the necessary boundary conditions, though the latter are not clearly stated in the published literature. For a comprehensive review of mathematical modeling of liquid–liquid extraction columns, their advantages and disadvantages, the interested reader could refer to Mohanty (2000).

The application of the population balance approach is expected to provide invaluable information if no careful modeling of the breakage and coalescence, as well as droplet transport laws, is taken into consideration. However, due to the recent extensive research for determining the kinetics of droplet breakage and coalescence as well as droplet transport from single and swarm droplet experiments, it becomes more possible than before to introduce more realistic models for these kinetic parameters and the transport laws (Cauwenberg et al., 1997; Kentish et al., 1998; Colella et al., 1999; Modes, 2000; Alopaeus et al., 2002; Biggs and Lant, 2002; Bart, 2003; Desnoyer et al., 2003; Mignard et al., 2003). Actually, this detailed level of information is at the expense of the mathematical complexity and thus demands a high computational cost since no analytical solution is known for the general population balance equation. Consequently, a numerical solution is required if precise simulation of the dispersed phase processes is required. In the last two decades there are many published papers concerned with the numerical solution of many special cases of the PBE arising from the modeling of many chemical and physical processes (Gelbard and Seinfeld, 1978; Sastry and Gaschignard, 1981; Gelbard et al., 1980; Casamatta and Vogelpohl, 1985; Al Khani et al., 1988, 1989; Hounslow et al., 1988; Marchal et al., 1988; Guimaraes et al., 1992; Hounslow, 1990; Kronberger et al., 1994; Hill and Ng, 1995, 1996, 1997; Kronberger et al., 1995; Ribeiro et al., 1995, 1997; Zimmermann et al., 1995; Kumar and Ramkrishna, 1996a,b, 1997; van Peborgh Gooch and Hounslow, 1996; Zamponi et al., 1996; Liou et al., 1997; Song et al., 1997; Nicmanis and Hounslow, 1998; Toutain et al., 1998; Vanni, 1999, 2000; Lee et al., 2001; Wulkow et al., 2001; Bennett and Rohani, 2001; Liu and Cameron, 2001; Motz et al., 2002; Lim et al., 2002; Verkoeijen et al., 2002; Mahoney and Ramkrishna, 2002; Diemer and Olson, 2002a,b; Attarakih et al., 2003a,b; Campos and Lage, 2003; Goodson and Kraft, 2003). Despite this intensive research, no general numerical approach exist which is applicable to the general PBE when multivariate population distributions are necessary to be taken into account. The dependence of the average number distribution on droplet size, concentration and perhaps age (Ribeiro et al., 1995; Gerstlauer, 1999) is an example of such multivariate distribution in liquid–liquid dispersions. Moreover, the problem becomes more complicated when external coordinates appear as in the case of differential population balance models. By external coordinate it is meant the physical space (continuous phase) which is occupied by the droplets and hence it is distinguished from the internal coordinates describing the droplet properties such as size, concentration, age, etc. (Hulburt and Katz, 1964). This independent set of coordinates is often referred to in the population balance literature as the droplet (particle) phase space. One attractive approach to reduce the dimensionality of the population balance equation is by averaging it with respect to selected internal coordinate through the use of the method of moments (Diemer and Olson, 2002a,b). The method of moments is considered very attractive from computational point of view especially when specific average properties of the population are the target of the calculations. Unfortunately, the

method of moments is not without inherent problems due to the closure and the distribution reconstruction intricacies (Diemer and Olson, 2002a,b).

1.1. Review of the available numerical methods

Apart from the method of moments, the most frequently used numerical methods for the solution of the PBE could be grouped into three categories: stochastic, higher-order and zero-order methods.

1.1.1. Stochastic methods

Stochastic approaches as differentiated from finite difference methods are simulation techniques designed to artificially realize the system behavior through the generation of random numbers used for the identification of the probability functions governing the system behavior (Ramkrishna, 2000). This stochastic simulation approach has the advantage of being capable of simulating the multivariate PBE with respect to internal coordinate when the other numerical methods become extremely expensive. A presentation of two currently used algorithms for stochastic simulation of the PBE in a batch stirred tank: the direct simulation and the mass flow algorithms is found in Goodson and Kraft (2003).

1.1.2. Higher-order methods

Most of the higher-order methods try to approximate the distribution function by a set of linearly independent functions of order greater than zero through the finite element method. Gelbard and Seinfeld (1978) solved the PBE for droplet coalescence in batch stirred tank using the orthogonal collocation on finite elements with cubic polynomials and by scaling the droplet diameter logarithmically. Nicmanis and Hounslow (1998) solved the PBE for continuous stirred tank at steady state using the mixed Galerkin and the orthogonal collocation methods on finite elements with cubic polynomials. Despite their accuracy, the major disadvantage of these methods is the excessive computational load imposed by evaluation of double integrals. This is particularly when the breakage and coalescence functions are dependent on some integral property associated with the population such as the dispersed phase hold-up (time dependent). Mahoney and Ramkrishna (2002) addressed this issue in addition to the difficulties associated with singularities of the integrand where suggestions are presented to remove these singularities for specific coalescence frequencies. Wulkow et al. (2001) solved the PBE for crystallization process using the Galerkin method on finite elements, which is adaptive in both droplet size and order (Galerkin-h-p). Hamilton et al. (2003) used the orthogonal collocation method using the Hermite basis functions weighted with the log-normal distribution. Their numerical results showed that the method is very accurate; however, at the expense of computational cost due to the appearance of many double integrals in the source terms. The major draw back of these methods like the other weighted residual-based methods is the difficulty to decouple the time-dependent frequencies (coalescence and breakage) from the time-dependent variables, and hence the computational cost is increased excessively especially when more than one coordinate in the PBE is involved. An extensive review of these methods could be found in Ramkrishna (1985, 2000).

1.1.3. Zero-order methods

Zero-order methods as referred to by Kostoglou and Karabelas (1994, 1995) are methods concerned with representing the population distribution after dividing the droplet size into finite number of classes by a constant value (zero-order polynomial) in each class. In this way the original integro-partial differential equation is transformed into a system of ODEs for which the numerical solution is well established. Zero-order methods could be classified into two broad classes according to Kumar and Ramkrishna (1996a): internally consistent and inconsistent discretization schemes with respect to selected integral properties. By internal consistency it is meant that the desired integral property associated with the average number concentration obtained from the discrete PBE should be the same as that obtained from its continuous counterpart. This internal consistency is found to predict accurately the desired integral properties and at the same time improves the accuracy of the predicted droplet distribution on coarse grids (Hounslow et al., 1988; Lister et al.,1995; Kumar and Ramkrishna, 1996a,b; Attarakih et al., 2003a,b). Hounslow et al. (1988) were the first who introduced an internally consistent set of discrete PBEs with respect to total number and volume for droplet coalescence in batch stirred tank using a geometric grid of constant factor 2. Unfortunately, this method is not amenable to grid refinement and it was extended to variable geometric factor by a set of more complicated discrete equations by Lister et al., 1995. Hill and Ng (1995, 1996) followed this line and derived a discretized PBE for droplet breakage and coalescence in a batch stirred tank with a major flaw that it is dependent on the type of the breakage functions for droplet breakage and the type of the grid for droplet coalescence. Their simple extension to continuous stirred tank is considered internally inconsistent, as we will show in this work. One of the earliest works to force internal consistency by conserving total droplet number and volume is presented in the paper by Sastry and Gaschignard (1981). These authors introduced two coupled sets of discrete PBEs for droplet coalescence in terms of number and volume balances with the appearance of double integrals in the source and sink terms and thus showing an excessive computational costs. Kumar and Ramkrishna (1996a) used the advantage of internal consistency and introduced a general framework of zero order discretization that is internally consistent with respect to any two integral properties irrespective of the grid structure. This scheme is called the fixed-pivot technique because it concentrates the droplet population in a given size range at a

single point (called the pivot) through the use of Dirac delta function. The underlying idea in this approach is that when a droplet is formed by either breakage or coalescence on a discrete grid its resulting characteristic volume will never coincide with any of the representative volumes except for the linear grid (with respect to droplet volume). In the classical discretization approaches the resulting droplet volume is assigned to the nearest pivot and hence it could be shown that only one integral property could be conserved (Attarakih et al., 2004). To conserve at least two integral properties the resulting droplet volume is linearly interpolated between two adjacent pivots so that any two integral properties are conserved. The fixed-pivot technique is found to be very powerful not only in predicting the unimodal but also the bimodal distributions when the other zero-order methods fail to do that or become computationally expensive (Vanni, 2000). Another variation of this approach is introduced by the same authors (Kumar and Ramkrishna, 1996b) making use of the idea of Sastry and Gaschignard (1981) and that of internal consistency through the so-called moving-pivot technique. For example when both total number and mass are the desired quantities to be conserved, the technique results in two sets of number and volume balances coupled through the pivots. These pivots are now dynamic quantities and change their positions to reflect the changes in the average number distribution. Attarakih et al. (2003a) extended recently the moving-pivot technique to a continuous stirred tank with only droplet breakage. Despite the high accuracy of the scheme it is considered computationally expensive when applied to PBEs showing spatial variation of the distribution. Lee et al. (2001) exploited the advantages of the fixed-pivot technique and coupled it with an adaptive mesh method and the method of characteristics to simulate a batch crystallizer of potassium sulfate. Lim et al. (2002) also made use of the fixed-pivot technique and weighted essentially non-oscillatory (WENO) scheme applied to the growth term to solve the PBE for a batch crystallizer of potassium sulfate. Although these authors claimed that their method conserves the total crystal number and mass, the discrete equations for agglomeration and breakage they used conserve only the total number due to the erroneous expressions resulting when the size coordinate is transformed from mass to length. Most recently, Campos and Lage (2003) have also used the fixed-pivot technique in the simulation of a bubble column through a mixed Euler–Lagrangian formulation. However, they failed to take into account the problem of internal consistency due to the presence of the feed distribution. This means that the extension of either the fixed-pivot or moving-pivot techniques to continuous flow systems is not simply by plugging the discrete equations of the source term in the model. In our previous work (Attarakih et al., 2003a) we have shown how the moving-pivot technique could be *correctly* extended to continuous flow systems.

It is worthwhile to mention some of the internally inconsistent methods such as the Galerkin method on finite elements with zero-order polynomials (Kronberger, 1995), the finite difference method of Ribeiro et al. (1995) and the wavelet-based method presented by Liu and Cameron (2001). The first method was introduced to discretize the PBE describing the hydrodynamics of liquid–liquid extraction columns. The method is not only less accurate than the fixed-pivot technique, but also it is computationally less efficient due to the many double integrals in the source term. Ribeiro et al. (1995) presented a simple first-order finite difference scheme for both droplet size and time to simulate the hydrodynamics of a continuous stirred tank. The algorithm is also extended to three internal coordinates: droplet volume, age and concentration where the method is only consistent with respect to total droplet volume (Ribeiro et al., 1997). The wavelet-based method is used to discretize the PBE by approximating the average number concentration and the coalescence frequency using a series of wavelets. Liu and Cameron (2001) reported that the resulting computational matrices resulting from the wavelet collocation algorithm are computed offline for time-independent coalescence frequencies. The method is shown to have good prediction of the average number concentration and its associated moments when sufficient number of collocation points are used (greater than 67 for the case of constant coalescence frequency). The method was only compared to some analytical solutions and not with any competing approach for the solution of the PBE to assess its performance. Bennett and Rohani (2001) used the combined Lax–Wendroff and Crank–Nicholson methods to simulate an evaporative cooling crystallizer with fines dissolution. The convergence and accuracy of the method for general cases including breakage and coalescence were not considered. Motz et al. (2002) applied the space-time conservation element and solution element (CE/SE) (Chang et al., 1999) to crystallization process with only crystal growth, attrition, dissolution and nucleation. Their numerical results for crystal growth simulation showed that this method is much superior to a second-order flux-limited upwind scheme (Koren, 1993), however; the method was not extended to include crystal agglomeration or breakage.

Compared to the above mentioned literature concerning the solution of the PBE of one internal coordinate, there is a few numbers of numerical studies with regard to PBE showing external coordinate dependency when interacting liquid–liquid dispersions are considered. For the numerical solution of stagewise models the interested reader could refer to Gerstlauer (1999) and Mohanty (2000). For differential PBE models, Al Khani et al. (1988), Gourdon and Casamatta (1994) and Milot et al. (1990) used the finite difference methods for discretizing both the internal and external coordinate; however, they presented no detailed information about the algorithms. Milot et al. (1990) reported that the spatial finite difference scheme that he used shows spurious numerical oscillations unless fine grid is used around the dispersed and continuous phase inlets. Kronberger et al. (1994, 1995) solved the PBE with spatial dependency using the

Galerkin and the finite volume methods for discretization of the internal and external coordinates respectively. The resulting discrete set of PBEs was treated as a system of conservation laws. They used a first-order upwind scheme with flux vector splitting based on the sign of the local droplet velocity. However, the approximate Riemann solver of Roe they used requires the estimation of the eigenvalues of the convective flux Jacobian, which is computationally very expensive for large systems. At a steady state where mild gradients exist they reported that both schemes produced identical results. Moreover, the aforementioned authors used a limited flux-extrapolation scheme of second-order accuracy. In spite of limiting the numerical flux it still shows spurious oscillations at the dispersed phase inlet especially during the transient period where large gradients are expected to occur.

Apart from interacting liquid–liquid dispersions, recently Campos and Lage (2003) presented a mixed Euler–Lagrange formulation for solving the PBE of a bubble column including bubble breakage, coalescence and absorption. They considered only positive bubble velocities and used third order total variation diminishing (TVD) scheme to discretize the convective term.

In this work we have developed a numerical algorithm to solve the PBE describing the hydrodynamics of interacting liquid–liquid dispersions showing both spatial and time dependencies as well as droplet interactions (breakage and coalescence). The underlying idea of this work is presented briefly by Attarakih et al. (2003b) and will be extended, numerically tested and experimentally validated in this work. From the literature review above, it is clear that the fixed-pivot offers the advantages of being relatively simple, accurate and computationally efficient and hence it will be *correctly* extended and efficiently applied to continuous flow systems. Unlike, the previous works reported for spatial discretization, which usually use upwind differencing schemes, we utilize a couple of first and second order accuracy central differencing schemes recently developed by Kurganov and Tadmor (2000). These schemes offer the advantage over the upwind schemes that they are free of any approximate Riemann solvers and hence are not tied to the eigenvalue structure of the Jacobian of the convective flux. In addition to these two central schemes a simple first-order upwind differencing scheme with flux vector splitting is derived based on the transport phenomena of the dispersed phase in a general liquid–liquid extraction column. The remaining body of the paper is arranged as follows: in Section 2 we present the general PBE for continuous flow systems and then it is simplified to the special case of a differential liquid–liquid extraction column (LLEC). The generalization of the fixed-pivot technique to continuous flow systems will be presented in Section 3 by stressing how the feed source term is treated. In this section, the coalescence and breakage matrices are restructured to improve the scheme performance with special attention paid to the finite domain error. In Section 4 we derive the semi-discrete PBEs based on the LLEC transport and the interactions of the dispersed and continuous phases along with the introduction of the central first- and second-order semi-discrete schemes, as well as the time discretization of the resulting system of ODEs. In Section 5 we validate the algorithm by presenting three analytical solutions of the simplified PBE for LLECs against which the full discretization of the PBE is tested. The experimental realization of the model is dealt with in Section 6 by considering a laboratory scale LLEC of rotating disc type (RDC) for which the steady-state hydrodynamic experimental data are available (Modes, 2000). Finally in Section 7 we present our conclusions and recommendations.

2. The general population balance equation

The PBE describing the hydrodynamics of a dispersed phase flowing in a continuous flow system in the absence of other transport phenomena such as mass transfer (no convective flux along the droplet internal coordinate) could be written as

$$\frac{\partial n(v;\boldsymbol{r},t)}{\partial t}+\nabla\cdot\boldsymbol{F}=\nabla\cdot(\boldsymbol{D}_d\nabla n)+\rho\{n,v\}, \tag{1}$$

where v is the droplet volume, $\boldsymbol{r}=[x,y,z]$, is a vector of external coordinate specifying the spatial variation of n. $n(v;\boldsymbol{r},t)\partial v=N(t,\boldsymbol{r})f(v)\partial v$ is the average number concentration associated with droplets having a volume between $v\pm\partial v$ at the time instant t and position in space $\boldsymbol{r}$ and its corresponding total number concentration is $N(t,\boldsymbol{r})$ while $f(v)$ is the average number density. The second term on the left-hand side represents the droplet transport by convection through surface of a given volume in space with velocity $\boldsymbol{U}_d=[U_{d,x},U_{d,y},U_{d,z}]$ and flux $\boldsymbol{F}=\boldsymbol{U}_d n$. The first term on the right-hand side is the droplet transport by diffusion characterized by the random movement of the individual droplets, in contrast to the convective transport by the turbulent eddies. The coefficient $\boldsymbol{D}_d$ appearing in this term is the Fick's diffusion tensor. The last term on the right-hand side is the net number of droplet produced by either breakage or coalescence per unit time and unit volume and is given by (Valentas and Amundson, 1966)

$$\begin{aligned}\rho\{n,v\}&=-\Gamma(v,\phi)n(v;z,t)\\&\quad+\int_v^{v_{\max}}\Gamma(v',\phi)\beta_n(v|v')n(v';z,t)\partial v'\\&\quad-n(v;z,t)\int_{v_{\min}}^{v_{\max}-v}\omega(v,v-v',\phi)n(v-v';z,t)\partial v'\\&\quad+\frac{1}{2}\int_v^{v_{\max}}\omega(v,v-v',\phi)n(v-v';z,t)n(v';z,t)\partial v'.\end{aligned} \tag{2}$$

The first and third terms in the above expression represent the rate at which the droplets are lost by breakage and coalescence per unit volume, respectively, while the second and the fourth terms account for the rate of formation of droplets by breakage and coalescence per unit volume, respectively. The breakage and coalescence frequencies are given by the

functions, Γ and ω, respectively, and are dependent on the agitation intensity, the system physical properties, the internal column geometry and the dispersed phase hold-up that is given by

$$\left(\phi(\boldsymbol{r},t)=\int_{v_{\min}}^{v_{\max}} vn(v;\boldsymbol{r},t)\partial v\right). \tag{3}$$

Note that the function $\beta_n(v|v')$ represents the distribution of the daughter droplets, given that a mother droplet of volume v' is broken and is assumed independent of time, but it may be function of the energy input and the system physical properties. This function should satisfy the usual number, volume and the physical ($\beta_n(v|v')=0,\ v>v'$) constraints (Ramkrishna, 2000).

2.1. The PBE for a differential LLEC

The PBE for a countercurrent LLEC without mass transfer and showing spatial variation only along the column height could be simply deduced from Eq. (1):

$$\frac{\partial n}{\partial t}+\frac{\partial F}{\partial z}=\frac{\partial}{\partial z}\left(D_d\frac{\partial n}{\partial z}\right)+\frac{Q_d}{A_c}\left(\frac{n^{\text{feed}}}{v_f}\right)\delta(z-z_d)+\rho\{n,v\}, \tag{4}$$

where $n(v;z,t)\partial v=N(t,z)f(v)\partial v$ is the average number concentration of droplets having a volume between $v\pm\partial v$ at the time instant t and column height z, and $N(t,z)$ is the total number concentration. The convective flux of these droplets along the column of a constant cross sectional area, A_c is represented by $A_cF\partial v=A_cU_dn\partial v$, where U_d is the velocity of the dispersed phase relative the column walls and will be derived later on. The first term on the right-hand side of Eq. (4) represents the axial dispersion of the dispersed phase due to the non-ideal flow in which a random movement of the fluid on the microscopic level is superimposed on the main flow (Zhu et al., 1984). This is assumed to follow Fick's law with a diffusion coefficient, D_d, and is distinguished from the forward mixing effect due to the droplet velocity distribution that is taken into account by the convective term (Zhang et al., 1985). The second term on the left-hand side represents a number concentration rate of droplet entering as a feed of volumetric flow rate, Q_d, at the level z_d of the column. The positive direction of flow coincides with the dispersed phase flow from z_d to the top of the column. Note that the feed distribution is represented mathematically by a point source through the use of the Dirac delta function (Kronberger et al., 1994).

It should be noted that Eq. (4) is unlike the previous PBE models that are written directly in terms of volume rather than number concentration (e.g. Casamatta and Vogelpohl, 1985; Kronberger et al., 1994), since the internally consistent discrete PBEs in terms of any desired quantity are always derived from the number concentration PBE. Moreover, Eq. (4) is written in terms of the droplet volume rather than diameter as the internal coordinate to eliminate the complex expressions resulting from the internal coordinate transformation. However, we will simply project back the discrete PBEs onto the droplet diameter coordinate using the identity:

$$\int_{v_{i-1/2}}^{v_{i+1/2}} n(v;z,t)\partial v=\int_{d_{i-1/2}}^{d_{i+1/2}} n(d;z,t)\partial d. \tag{5}$$

The boundary conditions are greatly simplified since the dispersed and the continuous phases are included in the model as point sources. So, the Danckwart's boundary conditions based on the discussion of Wilburn (1964) could be written by considering the LLEC to behave like a closed vessel between 0^+ and column height H:

$$0=\max(F,0)-D_d\frac{\partial n}{\partial z}\quad \text{at } z=0, \tag{6}$$

$$0=-\min(F,0)+D_d\frac{\partial n}{\partial z}\quad \text{at } z=H, \tag{7}$$

$$n(v;z,t)=n_0(v;z)\quad \forall z\in[0,H]. \tag{8}$$

The first boundary condition satisfies the continuity of the dispersed phase flux taking into account the possibility of droplet entrainment with the countercurrent continuous phase. The second boundary condition idealizes the situation at the top interface and simply means that the droplets with positive rise velocity reaching the level, H, will leave the column. However, realistic modeling of the mechanism of droplet coalescence at the interface needs more hydrodynamic considerations (Hartland and Jeelani, 1994).

In the above formulation, we also assume that the droplet breakage and coalescence are active only for $\forall z\in[z_d,z_c]$ and zero otherwise, where z_c is the continuous phase inlet. are applicable for this case. In addition to the initial condition implied by Eq. (8), the mathematical model given by Eq. (4) is also subjected to the regulatory conditions: $n(v<v_{\min},t)=0$ and $n(v>v_{\max},t)=0$.

2.1.1. The dispersed and continuous phase velocities

The droplet rise velocity of the dispersed phase relative to the continuous one is given by

$$U_r(d,z,\phi)=U_d\pm U_c, \tag{9}$$

where the plus sign stands for countercurrent flow systems and the negative one stands for cocurrent systems. U_d and U_c are the actual dispersed and continuous phase velocities with respect to the column walls, respectively. The relative velocity (also called the slip velocity) may be found from the single droplet terminal velocity modified such that the effect of the droplet swarm and the slowing effect due to the column internals are taken into account. Unfortunately, the form of this velocity is found dependent on the type of the column as well as the system physical properties. For comprehensive review of the slip velocity, as well as a simple guide for choosing the terminal droplet velocity, the reader could refer to Gourdon and Casamatta (1994). Nevertheless, we will assume a quite general form of the relative velocity so that it could be simply adapted to the type

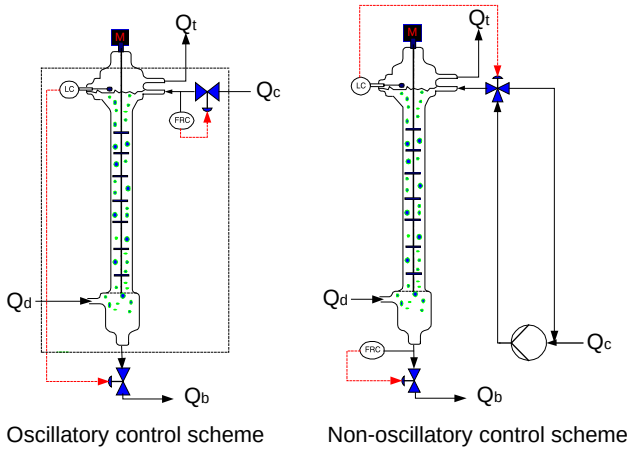

Fig. 1. Conventional and improved dispersed phase level controls (Hufnagl et al., 1991).

of the column and the chemical system under investigation:

$$U_r(d,z,\phi) = K_v U_t(d,\boldsymbol{P}) f(\phi). \tag{10}$$

In the aforementioned equation K_v is droplet slowing factor having a value between zero and one which takes into account the internal column geometry and might be dependent on energy input, and the droplet diameter (Modes, 2000). U_t is the single droplet terminal velocity and is adequately described by some correlation such as Klee and Treybal (1956), Vignes (1965) and Grace et al. (1976) depending on the system physical properties (Gourdon and Casamatta, 1994). The function $f(\phi)$ takes into account the effect of droplet swarm and is generally taken as $(1-\phi)^m$, where m is an empirical exponent (Godfrey and Slater, 1991), while the vector $\boldsymbol{P}$ may consist of all the system physical properties.

The remaining unknown in Eq. (9) is the continuous phase velocity which is usually determined in either two ways: The first one is due to Casamatta (1981) which is derived by making a total volume balance around a closed control volume spanning the column height from the base to an arbitrary level z. The derivation is accomplished by assuming that the variation of the continuous flow rate and hence U_c will cause an immediate change to the flow of the continuous phase. Kronberger (1995) presented a more mathematically sound derivation of this velocity model by coupling the dispersed and the continuous phases balances. This velocity model is valid at each instant of time and hence is suitable to transient column simulations although it shows oscillatory behavior in the transient hold-up due to the perfect control of the interface at the upper settling zone as shown in Fig. 1. The second velocity model is simpler than the first one and is derived by assuming the continuous phase hold-up at a steady state and hence it is valid only for steady-state simulations (Kronberger, 1995). The first model will be denoted as the oscillatory velocity model and the second one as a steady-state velocity model, where both models are presented in Table 1 for the sake of clarity.

Hufnagl et al. (1991) tried to improve the prediction of their lumped hydrodynamic model, which was unable to follow the oscillatory experimental hold-up behavior by suggesting an elegant interface level control scheme that proved experimentally to eliminate the transient oscillatory behavior of the dispersed phase hold up. However, their idea was not mathematically formulated until 1998 when Weinstein et al. (1998) included this idea in their lumped hydrodynamic model for a Kuhni LLEC. The stagewise dynamic population balance model of Gerstlauer (1999) was also neither able to follow the oscillatory behavior of the hold up experimental profile nor to correctly eliminate it. The reason is simply that this author used the steady state continuous phase velocity model described above.

Accordingly, we present below an improved non-oscillatory continuous velocity model based on the control scheme of Hufnagl et al. (1991). The idea of these authors is to manipulate the inlet continuous feed flow rate rather than the traditional manipulation of the outlet continuous flow rate (see Fig. 1). Now applying total volume balances around the control volume indicated by the dashed line in Fig. 1 we get the following two relations:

$$Q_{c,\mathrm{in}} + Q_d = Q_t + Q_b \tag{11}$$

and note that

$$Q_{c,\mathrm{out}} = (1-\phi_e)Q_b, \tag{12}$$

Table 1
Available continuous phase velocity models

Continuous phase velocity model	Reference
1. Oscillatory: $U_c = \frac{Q_t}{A_c} - \alpha_c \frac{Q_{c,\mathrm{in}}}{A_c} - \alpha_d \frac{Q_{d,\mathrm{in}}}{A_c} - \int_{d_{\min}}^{d_{\max}} v(d) U_r(d,\phi,P) n(d;z,t)\delta d$	Casamatta (1981)
2. Steady state: $U_c = \alpha_c \frac{Q_c}{A_c(1-\phi)} + \frac{D_c}{1-\phi}\frac{\partial\phi}{\partial z}$	Kronberger (1995)
$Q_t = \int_{d_{\min}}^{d_{\max}} v(d) U_r(d;\phi(H,t),\boldsymbol{P}) n(d;H,t)\delta d$	
$\alpha_c = \begin{cases} 1, & z \leqslant z_c \\ 0, & z > z_c \end{cases}$ and $\alpha_d = \begin{cases} 1, & z \leqslant z_d \\ 0, & z > z_d \end{cases}$	

where ϕ_e is the fraction of the dispersed hold up entrained with continuous phase if any. By combining the above relations we get the required continuous phase flow rate in terms of the dispersed phase throughput:

$$Q_{c,\text{in}} = Q_t + \frac{1}{1-\phi_e} Q_{c,\text{out}} - Q_d. \tag{13}$$

This equation, when combined with the oscillatory velocity model given in Table 1, it provides the improved non-oscillatory velocity model. Now the dispersed phase velocity, U_d, could be obtained directly from Eq. (9) and hence the hydrodynamic model of the LLEC is completely formulated.

3. Model discretization with respect to internal coordinate

The population balance model given by Eq. (4) represents a nonlinear integro-partial differential equation (IPDE) of convective-diffusion type, where the source of nonlinearity is due to the convective and the source terms. To project this IPDE onto a finite set of PDEs, we discretize the droplet internal coordinate, v, according to the following discrete set: $\{v_{i-1/2} | i = 1,\ldots,M_x+1\}$ with $v_{\min} = v_{1/2} < v_{3/2} < \cdots < v_{M_x+1/2} = v_{\max}$. Let the ith subdomain be defined as $V_i = [v_{i-1/2}, v_{i+1/2})$, $i = 1,\ldots,M_x$ and the population of the ith subdomain be concentrated at the middle of this subdomain so that $x_i = (v_{i-1/2} + v_{i+1/2})/2 = \pi d_i^3/6$ (see Fig. 2). Then the droplet size distribution is expanded using a point wise sampling of the distribution at the middle of the ith subdomain (also called the pivot) according to the following relation:

$$n(v;z,t) = \sum_{i=1}^{M_x} N_i(z,t)\delta(v - x_i), \tag{14}$$

where δ refers to the Dirac delta function and the set of the unknown coefficients, $N_i(z,t)$, refer to the total number concentration in the ith subdomain. Let us define the total quantity of droplets associated with a single droplet property $u_m(v)$ in the ith subdomain by:

$$I_i(z,t) = \int_{v_{i-1/2}}^{v_{i+1/2}} u_m(v) n(v;z,t)\partial v = u_m(x_i) N_i(z,t), \quad m = 1,2, \tag{15}$$

where the volume fraction, $\varphi_i(z,t)$, and the total number of droplets in the ith subdomain, $N_i(z,t)$, follow directly by substituting $u_2(v) = v$ and 1, respectively, in the last equation.

Kumar and Ramkrishna (1996a) showed that when the source term given by Eq. (2) is discretized by integrating it from $v_{i-1/2}$ to $v_{i+1/2}$ with respect to v, the source of internal inconsistency as described in Section 1.1.3 results mainly due to the formation terms of breakage and coalescence but not due to the loss terms. They solved this problem through modifying the formation terms due to breakage and coalescence by multiplying them with a triangular function that we may define as

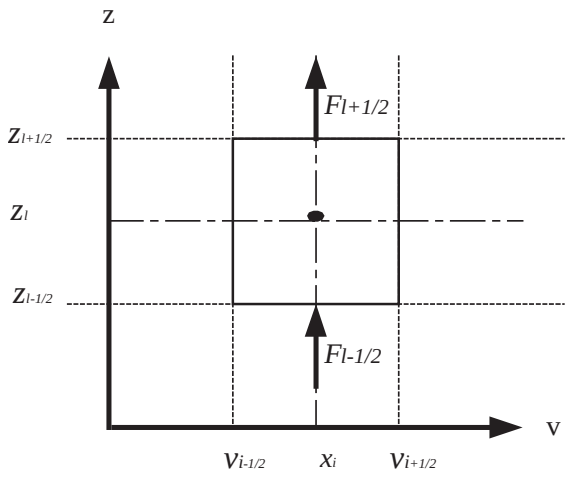

Fig. 2. External and internal coordinates discretization cell.

$$w_i(v) = \begin{cases} \gamma_i^{\langle i-1\rangle}(v), & x_{i-1} \leqslant v < x_i, \\ \gamma_i^{\langle i\rangle}(v), & x_i \leqslant v < x_{i+1}. \end{cases} \tag{16}$$

The set of linear functions, $\gamma_i^{\langle i-1\rangle}(v)$ and $\gamma_i^{\langle i\rangle}(v)$ should satisfy the constraints imposed by the conservation of any two integral properties associated with the number distribution function obtainable from those associated with the single droplet, $u_1(v)$ and $u_2(v)$:

$$\gamma_{i-1}^{\langle i-1\rangle}(v) u_m(x_{i-1}) + \gamma_i^{\langle i-1\rangle}(v) u_m(x_i) = u_m(v), \quad m = 1,2. \tag{17}$$

Making use of these ideas we can integrate Eq. (4) with respect to v from $v_{i-1/2}$ to $v_{i+1/2}$ with the aid of Eq. (14) and then multiply both sides by the general desired discrete quantity, $u_m(x_i)$, to get the following set of non-linear PDEs for a differential LLEC:

$$\frac{\partial I_i}{\partial t} + \frac{\partial F_i}{\partial z} = \frac{\partial}{\partial z}\left(D_d \frac{\partial I_i}{\partial z}\right) + \frac{Q_d}{A_c}\left(\frac{I_i^{\text{feed}}}{v_f}\right)\delta(z - z_d) + \rho_i\{\boldsymbol{I},\boldsymbol{d}\}, \tag{18}$$

where the source term for droplet breakage is transformed in terms of droplet diameter using Eq. (5) and is given by

$$\rho_{b,i}(\boldsymbol{I}) = -\Gamma(d_i,\phi(t,z))I_i + \sum_{k=i}^{M_x} \pi_{i,k}^{\langle m\rangle}\Gamma(d_k,\phi(t,z))I_k, \quad i = 1,2,\ldots,M_x, \tag{19}$$

$$\pi_{i,k}^{\langle m\rangle} = \int_{d_{i-1}}^{d_i} \gamma_i^{\langle i-1\rangle}(d)\left[\frac{u_m(d_i)}{u_m(d_k)}\right]\beta_n(d|d_k)\partial d + \int_{d_i}^{\min(d_k,d_{i+1})} \gamma_i^{\langle i\rangle}(d)\left[\frac{u_m(d_i)}{u_m(d_k)}\right]\beta_n(d|d_k)\partial d. \tag{20}$$

Note that the upper limit of integration on the second integral is set to satisfy the constraint: $\beta_n(d|d_k)=0,\ d \geqslant d_k$. Similarly, the source term for droplet coalescence could be written by introducing the idea of interaction coalescence matrix, $\boldsymbol{\Psi}$ as

$$\rho_{c,i}(\boldsymbol{I}) = \sum_{k=1}^{i}\sum_{j=k}^{i} \Psi_{k,j}^{\langle i\rangle}\omega_{k,j}I_kI_j - I_iu_m(x_i) \times \sum_{k=1}^{M\max(i)} \frac{\omega_{i,k}}{u_m(x_k)u_m(x_i)}I_k, \quad i=1,2,\ldots,M_x \tag{21}$$

where $\boldsymbol{d}=[d_1,d_2,\ldots,d_{Mx}]$, $\boldsymbol{I}=[I_1,I_2,\ldots,I_{Mx}]$ and the upper index on the loss term summation is the maximum integer so that: $M\max(i)=\max_k(d_i^3+d_k^3\leqslant d_{Mx}^3)$; $i,k=1,2,\ldots,M_x$.

The significance of introducing the coalescence interaction matrix has two distinctive advantages over the original formulation of Kumar and Ramkrishna (1996a). The first one is that this three-dimensional matrix is decoupled from the time-dependent variables, ω and $\boldsymbol{I}$ and hence it is always evaluated offline once a time. Second the ith coalescence interaction matrix, $\boldsymbol{\Psi}^{\langle i\rangle}$, has a size $i\times i\times i$ which grows linearly as i increases and hence this saves the storage requirement instead of storing an $M_x\times M_x\times M_x$ matrix for each i. This means that we only extract the ith interaction matrix from the $M_x\times M_x\times M_x$ matrix as we need it. Moreover, the sparse nature of the ith coalescence interaction matrix will reduce the execution time considerably, as we will see later. This is because we carry the above summations only when the resulting volume of any two droplets of volumes x_k and x_j falls in the ith subdomain. Thus, the nonzero elements in the ith coalescence interaction matrix are the volumes of the coalescing droplets that report in the ith subdomain and are given by

$$\boldsymbol{\Psi}_{k,j}^{\langle i\rangle} = \begin{cases} \left[1-\frac{1}{2}\delta_{k,j}\right]\frac{u_m(x_i)}{u_m(x_j)u_m(x_k)}\gamma_i^{\langle i-1\rangle}(x_k+x_k), \\ \text{if } d_{i-1}^3 \leqslant d_j^3+d_k^3 < d_{i-1}^3, \\ \left[1-\frac{1}{2}\delta_{k,j}\right]\frac{u_m(x_i)}{u_m(x_j)u_m(x_k)}\gamma_i^{\langle i\rangle}(x_k+x_k), \\ \text{if } d_i^3 \leqslant d_j^3+d_k^3 < d_{i+1}^3, \end{cases} \tag{22}$$

where $\delta_{k,j}$ is the kronecker delta.

The set of Eq. (18) is not internally consistent with respect to any two integral properties, $u_1(v)$ and $u_2(v)$ due to the presence of the feed distribution (Attarakih et al., 2004). The internal consistency could be restored if we generalize the fixed-pivot technique by considering the appearance of the feed distribution as a formation (birth) term similar to those for breakage and coalescence. Making use of this, we can multiply the feed distribution by the triangular function given by Eq. (16) and integrating with respect to v from $v_{i-1/2}$ to $v_{i+1/2}$ and then multiplying it by $u_m(d_i)$ to get

$$I_i^{\text{feed}} = \int_{d_{i-1}}^{d_i}\gamma_i^{\langle i-1\rangle}(d)[u_m(d_i)]f^{\text{feed}}(d)\partial d + \int_{d_i}^{d_{i+1}}\gamma_i^{\langle i\rangle}(d)[u_m(d_i)]f^{\text{feed}}(d|)\partial d. \tag{23}$$

Now it is with this final equation the set of Eq. (18) is internally consistent with respect to any two integral properties obtainable from its continuous counterpart given by Eq. (4).

3.1. Restructuring of the discrete source term

The recognition of the sparse structure of the coalescence interaction matrix makes it possible to reduce the computational time drastically. The first double summation in Eq. (21) recognizes only the triangular structure of the ith interaction coalescence matrix and ignores its sparse nature. This sparse nature is due to the definite number of droplets falling in the ith subdomain through coalescence of droplets from the kth and jth subdomians. Since not all the coalescence events will lead to droplet volumes falling in the ith subdomain, then a number less than or equal to $i(i+1)/2$ always exists representing the maximum number of droplets falling in the ith subdomain. So, before we initiate the calculations, we will determine a set of vectors and matrices: $K\min(i)$, $K\max(i)$, $M(i)$, $J\min(i,k)$, and $J\max(i,k)$ representing the locations of the non-zero elements of the ith interaction matrix once the grid structure becomes available. Hence, we modify the limits of the summations in the coalescence formation term as follows:

$$\rho_{c,i}(\boldsymbol{I}) = \sum_{k=K\min(i)}^{K\max(i)}\sum_{j=J\min(i,k)}^{J\max(i,k)} \Psi_{k,j}^{\langle i\rangle}\omega_{k,j}I_kI_j - I_iu_m(x_i) \times \sum_{k=1}^{M\max(i)} \frac{\omega_{i,k}}{u_m(x_k)u_m(x_i)}I_k. \tag{24}$$

Similarly the source term for droplet breakage could be written in terms of the breakage interaction matrix that have an upper triangular structure with the following elements:

$$A_{i,k} = \begin{pmatrix} [\pi_{i,i}^{\langle m\rangle}-1] \\ \pi_{i,k}^{\langle m\rangle} \end{pmatrix}, \quad i=1,2,\ldots,M_x, \quad k=i,\ldots,i+1,\ldots,M_x. \tag{25}$$

Like the coalescence interaction matrix it is independent of time and thus it is generated only once a time offline. The complete source term could now be written in a compact

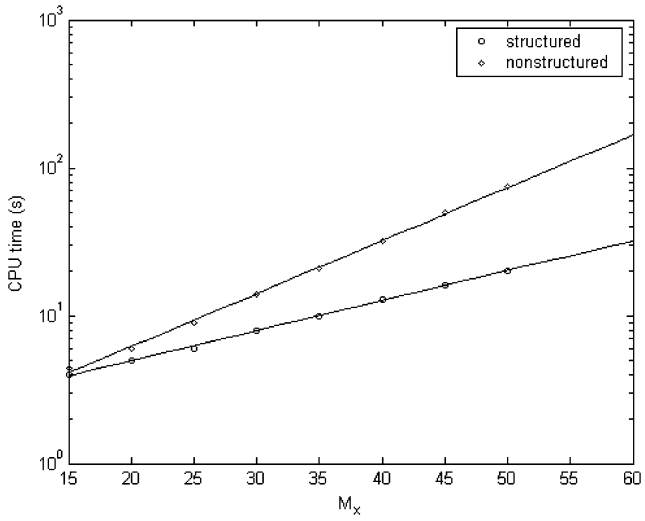

Fig. 3. The effect of restructuring the coalescence interaction matrices on the CPU time requirements for droplet coalescence in a continuous stirred tank. All the numerical runs are carried out using a PC of 750 MHz speed of type Pentium III and performing a single task with Compaq visual FORTRAN compiler version 6.6.

matrix form as follows:

$$\rho(\boldsymbol{I}) = \begin{pmatrix} \boldsymbol{I}^{\mathrm{T}}[(\boldsymbol{\omega}\cdot\boldsymbol{\Psi}^{\langle 1\rangle})\boldsymbol{I}] \\ \boldsymbol{I}^{\mathrm{T}}[(\boldsymbol{\omega}\cdot\boldsymbol{\Psi}^{\langle 2\rangle})\boldsymbol{I}] \\ \vdots \\ \boldsymbol{I}^{\mathrm{T}}[(\boldsymbol{\omega}\cdot\boldsymbol{\Psi}^{\langle M_x\rangle})\boldsymbol{I}] \end{pmatrix} - \boldsymbol{I}^{\mathrm{T}}\cdot[\boldsymbol{\omega}(\boldsymbol{\zeta}\cdot\boldsymbol{I})] + \boldsymbol{A}[\boldsymbol{\Gamma}\cdot\boldsymbol{I}], \tag{26}$$

where

$$\zeta_k = \frac{1}{u_m(x_k)} \tag{27}$$

and the symbol $\cdot$ appearing in Eq. (26) denotes an element by element matrix multiplication.

To see the effect of the above proposed restructuring, we simulated the case study presented by Hounslow (1990) for droplet coalescence in a continuous stirred tank. Fig. 3 shows the superior performance of the structured matrices when compared with the unstructured ones.

3.2. The finite domain error

Due to the presence of the boundary conditions (regulatory conditions) there would be an inevitable underestimation of the integral properties obtained from the number distribution if these boundary conditions are not exactly satisfied. This failure of taking into account the nonzero values of the portions of the distribution below $d_{\min}$, and above $d_{\max}$ (if these droplet sizes are not properly chosen) is termed the finite domain error (FDE) (Gelbard and Seinfeld, 1978; Nicmanis and Hounslow, 1998; Attarakih et al., 2003a). The subsequent erroneous estimation of $d_{\min}$, and $d_{\max}$ so that the regulatory conditions are not approximately satisfied, will result in an underestimation of the predicted integral quantities of interest. So, we present the following approximate relation to safely estimate the minimum and maximum internal coordinate sizes at fixed number of subdomians, M_x, so that the total FDE is below a specified tolerance TOL:

$$\mathrm{FDE}(d_{\min}, d_{\max}, M_x) = \mathrm{FDE}^L + \mathrm{FDE}^U \leqslant \mathrm{TOL}, \tag{28}$$

where

$$\mathrm{FDE}^L \approx \sum_{m=1}^{2}\sum_{i=1}^{2}\frac{1}{\Delta d_i}u_m(d_i)N_i(z,t) + \sum_{m=1}^{2}\sum_{i}^{2}\frac{1}{\Delta d_i}\left(\int_{d_{i-1/2}}^{d_{i+1/2}} u_m(d)n^{\mathrm{feed}}(d)\partial d + \int_{d_{i-1/2}}^{d_{i+1/2}} u_m(d)n^{ic}(d)\partial d\right), \tag{29}$$

$$\mathrm{FDE}^U \approx \sum_{m=1}^{2}\sum_{i=M_x-1}^{M_x}\frac{1}{\Delta d_i}u_m(d_i)N_i(z,t) + \sum_{m=1}^{2}\sum_{i=M_x-1}^{M_x}\frac{1}{\Delta d_i}\left(\int_{d_{i-1/2}}^{d_{i+1/2}} u_m(d)n^{\mathrm{feed}}(d)\partial d + \int_{d_{i-1/2}}^{d_{i+1/2}} u_m(d)n^{ic}(d)\partial d\right). \tag{30}$$

The derivation of these relations is shown in Appendix B.

Unfortunately, for a dispersed process in which both breakage and coalescence are active, the estimation of $d_{\min}$ and $d_{\max}$ has an iterative nature. First start with an initial estimation at fixed M_x, solve the complete problem, and check if the condition implied by Eq. (28) is satisfied. If it is not satisfied, then $d_{\min}$, will be reduced and $d_{\max}$ will be increased by a small amount and the problem is solved again until Eq. (28) is satisfied.

A particular advantage of this approach is that the above condition is checked at each integration step or perhaps at regular time steps and in each computational cell along the column. So, once this condition is violated the calculations should be stopped and restarted again with an improved estimation of $d_{\min}$ and $d_{\max}$. This reduces the computational time significantly while at the same time achieving an automatic FDE estimation. Moreover, another obvious advantage of the estimation of the total FDE is to minimize it at a specified simulation time by keeping the lower and upper finite domain errors approximately equal (Attarakih et al., 2003a).

4. Model discretization with respect to external coordinate

The discrete set of partial differential equations given by Eq. (18) is now in terms of any discrete quantity, $u_m(d_i)$

associated with the discrete number concentration, $N_i(z,t)$. The question that presents itself at this stage is, which discrete quantity, $u_m(d_i)$ that is suitable for the discretization of Eq. (18) with respect to the external coordinate? This question might be answered if we are guided by the volume approach for the PBEs presented recently by Verkoeijen et al. (2002). These authors have pointed out that the volume distribution based on droplet volume as an internal coordinate is the most suitable when the PBE is coupled with a fluid dynamics model as in our case. This volume distribution becomes inevitable since the finite volume numerical approach is the most feasible one for external coordinate discretization for the system of PDEs given by Eq. (18) (Toro, 1999). This is because Eq. (18) represents a system of non-linear conservation laws coupled through the convective and source terms when the volume (mass) distribution is chosen to describe the droplet population evolution in space and time. It should not lead to confusion that the droplet diameter appearing in Eq. (18) contradicts the above conclusions since we projected the volume onto the diameter coordinate only after the internal coordinate discretization. Thus, we preserved all the advantages of using the droplet volume as internal coordinate discussed by Verkoeijen et al. (2002) such as the additive property of droplet volumes.

So, in the following section the finite volume numerical approach is used to discretize the PBEs with respect to the external coordinate (column height), using a volume distribution function by setting $u_1(v)=1$ and $u_2(v)=v$ in Eq. (15), which corresponds to the total droplet number and volume conservation.

4.1. Spatially first- and second-order discrete LLEC models

The system of conservation laws given by Eq. (18) is actually dominated by the convective term for typical values of D_d which are in the order of 10^{-4} m^2/s (Modes, 2000) (Peclet No. $\approx 1\times10^3\,H - 2\times10^3\,H$). Due to this and the presence of the point source term imposed by the feed at the location z_d it is expected that the total transient hold-up (and hence the hold-up of the different internal subdomains) will move along the column height with a steep front. Accordingly, high-resolution schemes are required to capture this moving front since first-order schemes are known to suffer from excessive numerical diffusion (front smearing) (Toro, 1999). However, it will be very useful in the first step of spatial discretization is to consider only a first-order accurate scheme which is based on droplet volume balance on discrete space (spatial cell). So recall that the ith convective flux is given by

$$F_i = U_d(d_i,\phi)\varphi_i(z,t) \tag{31}$$

and consider the general staggering spatial grid (cell-centered finite-volume approach) given in Fig. 2: $z_{l\pm1/2}= z_l \pm \Delta z_l/2$, $l=1,2,\ldots,L$ and let the average cell hold up be given as

$$\varphi_{i,l}(t) = \frac{1}{\Delta z_l}\int_{z_{l-1/2}}^{z_{l+1/2}} \varphi_i(z,t)\,\mathrm{d}z. \tag{32}$$

Now it is possible to consider the unsteady state droplet volume balance across the lth cell boundaries shown in Fig. 2 and the net volume (mass) generation of the dispersed phase in it. This cell volume could be considered small enough so that the spatial variation within it could be neglected. Since the droplet rise velocity, U_d, might be negative at any cell boundary due to the effect of the droplet swarm and/or the continuous phase velocity as indicated by Eq. (9), it is necessary to split the convective flux into negative and positive components:

$$F_{i,l+1/2} = F^+_{i,l} + F^-_{i,l+1}, \tag{33}$$

where

$$F^+_{i,l} = \max(U_i(d_i,\phi_l(t))\varphi_{i,l}(t),0), \tag{34}$$

$$F^-_{i,l+1} = \min(U_i(d_i,\phi_{l+1}(t))\varphi_{i,l+1}(t),0). \tag{35}$$

Note that the direction of these fluxes is from the bottom to top if positive and from the top to the bottom of the cell if negative, and only one flux at the same cell boundary exists. The total flux at the lth cell boundary me be extended to include the diffusive flux which is always positive in the direction of flow (Rice and Do, 1995) and hence

$$F^+_{t,i,l+1/2} = F^+_{i,l} - \frac{D_d}{2}\left.\frac{\partial\varphi_i}{\partial z}\right|_{l+1/2}, \tag{36}$$

$$F^-_{t,i,l-1/2} = F^-_{i,l} + \frac{D_d}{2}\left.\frac{\partial\varphi_i}{\partial z}\right|_{l-1/2}. \tag{37}$$

By applying the conservation of mass to the lth cell shown in Fig. 2 and making use of the fluxes definitions above, one could obtain the following set of ODEs:

$$\frac{\mathrm{d}\varphi_{i,l}}{\mathrm{d}t} + \frac{F_{i,l+1/2}-F_{i,l-1/2}}{\Delta z_l} = \frac{D_d(\partial\varphi_i/\partial z)_{l+1/2} - D_d(\partial\varphi_i/\partial z)_{l-1/2}}{\Delta z_l} + \frac{Q_d}{A_c}\frac{\varphi_i^{\mathrm{feed}}}{v_f}\frac{\delta_{l,l_d}}{\Delta z_l} + \rho(\boldsymbol{\varphi}_l,\boldsymbol{d}), \tag{38}$$

where $i=1,2,\ldots,M_x$, $l=1,2,\ldots,L$, and the spatial derivatives of the diffusive flux might be approximated as a difference between the centers of two adjacent cells where the hold-up values are known:

$$D_d\left.\frac{\partial\varphi_i}{\partial z}\right|_{l+1/2} \approx D_{d,l+1/2}\frac{\varphi_{i,l+1}-\varphi_{i,l}}{\Delta^* z_l}. \tag{39}$$

Note that $\Delta z_l = z_{l+1/2}-z_{l-1/2}$, which is the same as $\Delta^* z_l = z_{l+1}-z_l$ only for uniform spatial cells. Also note that the

discrete source term appearing in Eq. (38) is evaluated at the center of the lth spatial cell; that is, at $z = z_l$.

To complete the model, the discrete boundary conditions corresponding to Eqs. (8) and (9) could be easily written in terms of volume concentration as follows:

$$0 = F^{+}_{i,0} - D_d \left.\frac{\partial \varphi_i}{\partial z}\right|_{1/2} \quad \text{at } z = 0, \tag{40}$$

$$0 = -F^{-}_{L+1} + D_d \left.\frac{\partial \varphi_i}{\partial z}\right|_{L+1/2} \quad \text{at } z = H. \tag{41}$$

The discrete model given by Eq. (38) is an integral approximation to the system of conservation laws given by Eq. (18). This integral approximation exactly satisfies the conservation of volume and hence it presents no numerical difficulties (except its low accuracy) around the discontinuity caused by the feeds point sources. More interestingly, this model is exactly the same as that derived by Kronberger et al. (1995) and Kronberger (1995) based on first-order upwind differencing and flux vector-splitting scheme. This scheme as its name indicates uses the information available from grid points on the side from which the information flows. Thus for positive numerical flux the upwind side is the lower cell center and for negative flux the upwind side is the upper cell center. Despite the low accuracy of this scheme for unsteady state simulation it is stable, simple and accurate for steady state calculations where sharp profiles are not likely to occur. Moreover, the present semi-discrete scheme for a general LLEC could be easily related to the backflow-cell models by suitably relating the dispersion (diffusion) coefficient, D_d and the backflow fraction relative to the forward flow (McSwain and Durbin, 1966).

To circumvent the problem of numerical diffusion inherently existing in the first-order schemes, high-resolution schemes are required to lessen this numerical diffusion and hence sharpen the predicted moving front. This is done by increasing the order of spatial discretization of the numerical flux without violating the physical behavior of the phenomena under investigation. This violation comes from the fact that *linear* differencing schemes of order greater than one introduces spurious oscillation around large gradients according to the Godunov's theorem (Toro, 1999). Thus higher order upwind numerical fluxes are nonlinear and require more information by resorting to a complicated characteristic decomposition of the numerical flux more than the simplified approach presented above.

Recently, Kurganov and Tadmor (2000) presented a high-resolution central difference scheme of first- and second-order accuracy. These central differencing schemes offer universal black-box solvers for general systems of conservation laws such that given by Eq. (18). Moreover, the use of central differencing schemes in the presence of the diffusion as well as the source terms does not call for the operator splitting technique suffering from the traditional splitting limitations; that is, it requires a small time step, which is comparable to the diffusion time scale (Karlsen et al., 2001). Unlike the upwind differencing schemes, the central differencing schemes do not require the time-consuming characteristic decomposition called for by the approximate Riemann solvers (Toro, 1999). Additionally, the spatial numerical derivatives required for the high-resolution implementation could be evaluated in a componentwise manner in a way similar to the scalar nonlinear limiters. Similarly, the evaluation of the numerical flux Jacobian is not necessary, but instead the approximate flux derivatives are evaluated in a componentwise manner based on the neighboring discrete values of the numerical flux: $F(\varphi_{i,l-1}, \phi_{l-1})$, $F(\varphi_{i,l}, \phi_l)$ and $F(\varphi_{i,l+1}, \phi_{l+1})$.

The main idea behind these central differencing schemes is in the way which they evolve in time the reconstructed piecewise-polynomial values at the cell boundary from their known values at the cell centers. This evolution step is realized by sampling the reconstructed values at the cell boundaries by including more precise information about the local propagation speeds ($S_{l\pm1/2}$). Kurganov and Tadmor (2000) used these ideas to construct the following numerical flux approximation:

$$F_{i,l+1/2} = \frac{F(\varphi^{+}_{i,l+1/2}) + F(\varphi^{-}_{i,l+1/2})}{2} - \frac{S_{i,l+1/2}}{2}(\varphi^{+}_{i,l+1/2} - \varphi^{-}_{i,l+1/2}), \tag{42}$$

where

$$\varphi^{+}_{i,l+1/2} = \varphi_{i,l+1} - \frac{\Delta^{*} z_{l+1}}{2} \left.\frac{\partial \varphi_i}{\partial z}\right|_{l+1}, \tag{43}$$

$$\varphi^{-}_{i,l+1/2} = \varphi_{i,l} + \frac{\Delta^{*} z_l}{2} \left.\frac{\partial \varphi_i}{\partial z}\right|_{l} \tag{44}$$

and the propagation local speeds (irrespective of the direction of propagation) are estimated from the following relation:

$$\boldsymbol{S}_{l+1/2} = \max\left\{ r\left(\frac{\partial F(\boldsymbol{\varphi}^{-}_{l+1/2})}{\partial \boldsymbol{\varphi}}\right), r\left(\frac{\partial F(\boldsymbol{\varphi}^{+}_{l+1/2})}{\partial \boldsymbol{\varphi}}\right)\right\}, \tag{45}$$

where r denotes the spectral radius of the Jacobian matrix.

The spatial derivatives appearing in Eqs. (43) and (44) are evaluated using a minmod-like limiter (Kurganov and Tadmor, 2000) that is given by

$$\left.\frac{\partial \varphi_i}{\partial z}\right|_{l} = \text{minmod}\left(\theta \frac{\varphi_{i,l} - \varphi_{i,l-1}}{z_l - z_{l-1}}, \frac{\varphi_{i,l+1} - \varphi_{i,l-1}}{z_{l+1} - z_{l-1}}, \theta \frac{\varphi_{i,l+1} - \varphi_{i,l}}{z_{l+1} - z_l}\right), \quad 1 \leqslant \theta \leqslant 2, \tag{46}$$

where θ is a total variation diminishing (TVD) parameter with a value equals 2 corresponding to the least dissipative limiter, while the value of unity guarantees that the scheme is free from any spurious oscillations. For definition of the minmod limiter the reader could refer to Kurganov and Tadmor (2000).

Note that the above numerical flux (Eq. (42)) is of second order accuracy and could simply be made first order by setting the numerical derivatives in Eqs. (43) and (44) to zeros. Moreover, the estimation of the local propagation speeds, $S_{i,l\pm1/2}$, is carried out based on a crude estimation of the Jacobian so that its eigenvalues are approximately given by: $\lambda_i \approx U_{d,i}$, $i = 1,2,\ldots,M_x$ in a similar way as we did in Section 4.1 in Eqs. (34) and (35).

It is worthwhile to mention that the aforementioned numerical flux could be reduced exactly to that of Kurganov and Tadmor (2000) when uniform spatial grid is used.

4.2. Model discretization with respect to time

The semi-discrete model given by the set of ODEs (Eq. (38)) and the first-order upwind numerical fluxes appearing in Eqs. (33)–(37) as well as the central numerical fluxes given by Eqs. (42)–(46) admits the use of efficient time discretization schemes by contrast to its fully discrete versions. Although higher-order time differencing schemes offer high accuracy and time step control, they may violate the solution positivity, especially at high level of space discretization unless very small time steps are to be used. So, as a first simple time discretization, we apply the implicit Euler method by lagging the non-linear terms appearing in the convective and source terms. This discrete system could be written in a standard tridiagonal form in space for each internal coordinate subdomain and resolved using the standard Thomas algorithm at each time step followed by the fixed-point iteration method to improve the predicted solution due to lagging of the nonlinear terms. An accelerating convergence technique such as the bounded Wegstein method may be used. This iterative technique is only required for unsteady-state simulations, since for steady-state calculations the above algorithm converges always to the solution, irrespective of the time step size. Moreover, since the above tridiagonal system is diagonally dominant (Kronberger, 1995) with positive right-hand side, it is found to converge to the steady-state solution without any risk of having negative values ensuring the solution positivity.

5. Discrete model validation

The convergence and accuracy of the discrete models in both internal and external coordinates is tested in this section against analytical solutions whenever it is possible. Four case studies are considered of which three have analytical solutions that are derived in the present work. These three cases are for the LLEC model in which neither droplet breakage nor coalescence, only droplet breakage, and droplet coalescence alone with uniform dispersed phase velocity are considered. Case 4, which has no known analytical solution, considers a more practical situation where both breakage and coalescence mechanisms are active.

Table 2
RDC column geometry

Column diameter (m)	0.15	Column height (m)	2.550
Stator diameter (m)	0.105	Dispersed phase inlet (m)	0.250
Rotor diameter (m)	0.090	Continuous phase inlet (m)	2.250
Compartment height (m)	0.030		

In all the following results the average number or volume distributions are obtained using the following relation:

$$\bar{I}_i = \frac{u_m(d_i)N_i}{\Delta d_i}, \tag{47}$$

where $u_m(d_i)=1$ and $\pi d_i^3/6$ for the average number and volume concentrations, respectively, which are the conserved integral quantities according to the GFP. Consequently, the convergence tests are carried out based on the systematic error in terms of d30 as a mean droplet diameter. This choice of the mean droplet diameter includes the effect of both the conserved quantities on the error behavior. The systematic error is defined as

$$\text{SysErr} = |\text{d30}^a - \text{d30}^n|, \tag{48}$$

where the a and n superscripts on d30 refer to the analytical and numerical values, respectively.

In all the cases given below, unless explicitly stated, we discretized the droplet diameter logarithmically with lower and maximum droplet diameters were chosen so that the total FDE given by Eq. (30) is less than 0.1%:

$$d_{i-1/2} = d_{\min}\left(\frac{d_{\max}}{d_{\min}}\right)^{(i-1)/Mx}, \quad i = 1,2,\ldots,M_x+1. \tag{49}$$

In all the cases that follow we assumed zero initial condition at the instant where the dispersed phase feed is switched on. The column dimensions used in this work are that of a laboratory scale RDC column having geometrical specifications shown in Table 2. The chemical system used is the EFCE (European Federation of Chemical Engineering) test system: water-toluene for which the physical properties are available online (http://www.dechema.de/Extraktion). The spatial numerical schemes are denoted as follows: the first order upwind scheme with flux vector splitting is UW1FVS, the first- and second-order central differencing schemes of Kurganov and Tadmor (2000) are denoted by KT1 and KT2, respectively. The TVD parameter θ used in the reconstruction step of the KT2 method is set 1.7 as a compromise value between dissipative and oscillatory free solution behavior. Also, the two dimensional grid with respect to spatial and droplet diameter is denoted as $L \times M_x$, respectively.

5.1. Case 1: LLEC without breakage and coalescence

First we start solving the PBE given by Eq. (4) by dropping the diffusive and source terms, and we assume the dispersed phase is flowing through a stagnant continuous phase

($Q_c = 0$) at low hold-up such that the swarm effects are negligible. For the droplet terminal velocity the rigid sphere law interpolated between the viscous and inertial regions (Wesselingh and Bollen, 1999) is used:

$$U_t = \left[\left(\frac{g(\rho_c - \rho_d)d^2}{18\mu_c} \right)^{-0.85} + \left(\sqrt{\frac{1.74g(\rho_c - \rho_d)d}{\rho_c}} \right)^{-0.85} \right]^{-1/0.85}, \quad (50)$$

where the first term inside the brackets is simply the Stokes's law for viscous range and the second term is the droplet velocities in the inertial range and the various symbols are defined in the notation.

The analytical solution for this simplified PBE is obtained using Laplace transform with respect to time followed by solving the resulting linear ODE with respect to spatial coordinate. In terms of volume distribution $p(d;z,t)$, the analytical solution could be written as

$$p(d,z,t) = \frac{Q_d}{A_c U_t(d)}\, p^{\text{feed}} u(t - \tau(d,z)), \quad (51)$$

where

$$u(t - \tau(d,z)) = \begin{cases} 1, & t - \tau(d,z) \geqslant 0, \\ 0 & \text{otherwise}, \end{cases} \quad (52)$$

$$\tau(d,z) = \begin{cases} \dfrac{z - z_d}{U_t(d)}, & z - z_d \geqslant 0, \\ 0 & \text{otherwise}. \end{cases} \quad (53)$$

The inlet feed is taken as the Weibull distribution: $n^{\text{feed}} = \alpha\beta d^{\beta-1} e^{-\alpha d^{\beta}}$ with $\alpha = 1.1 \times 10^{-3}$ and $\beta = 8$. The minimum and maximum droplet diameters are 0.25 and 4.0 mm, respectively, $Q_d = 1.111 \times 10^{-4}$ m^3/s, and $\Delta t = 0.05$ s.

Fig. 4 shows the dispersed phase hold-up and the number concentration profiles at $t = 15$ s as compared to the analytical solution given by Eqs. (51)–(53). First, the two first-order upwind and central differencing schemes (UW1FVS and KT1) show identical predictions of the profiles on a two-dimensional grid of size 150 × 30. This is because it is easy to show that the central first-order scheme is reduced exactly to the first-order upwind scheme for linear convective problems. Due to their first-order accuracy the two schemes show numerical diffusion around the sharp moving front as expected. The use of the second-order central differencing scheme (KT2) eliminates almost the entire diffusing luggage accompanying the first-order schemes.

Fig. 5 shows the exact and numerical average volume distribution along the column height at $t = 15$ s using the KT2 scheme. The two solutions are almost identical and the forward mixing of the dispersed phase is also predicted. Large droplets travel faster than the small ones and hence they possess different residence times as it is observed experimentally (Zhang et al., 1985; Qian and Wang, 1992).

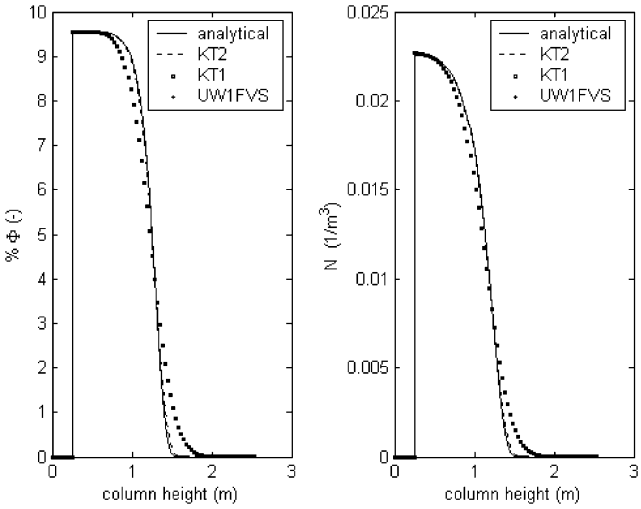

Fig. 4. Test of the spatial discretization algorithms using the simplified analytical solution of the PBE with grid dimensions: 150×30 (nonuniform and uniform grids) for internal and external coordinates, respectively, $t = 15$ s, $\Delta t = 0.05$ s, rigid sphere law terminal velocity, $Q_c = 0$ and $Q_d = 1.111 \times 10^{-4}$ m^3/s (case 1).

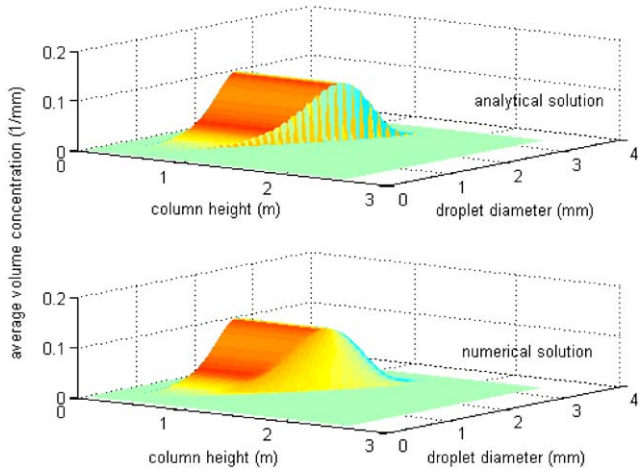

Fig. 5. Comparison of the numerical and exact transient behavior of the average volume concentration using the GFP and the second order central difference scheme (KT2) of case 1 with grid dimension: 150 × 30 for internal and external coordinates, respectively, $t = 15$ s, $\Delta t = 0.05$ s, $Q_c = 0$ and $Q_d = 1.111 \times 10^{-4}$ m^3/s.

Fig. 6 shows the transient total volume and number concentration profiles along the column using the KT2 scheme. First, the moving front is correctly tracked out when compared to the analytical solution given by Eq. (51). Second, the true volume and number concentration profiles are actually smearing as they move along the column due to the droplet forward mixing (different droplet velocities). This actually makes the numerical solution less difficult than predicting hypothetical profiles resulting from the uniform droplet velocity distribution as we will see in cases 2 and 3.

Fig. 7 shows the convergence characteristics of the central differencing schemes KT1 and KT2. It is clear that both

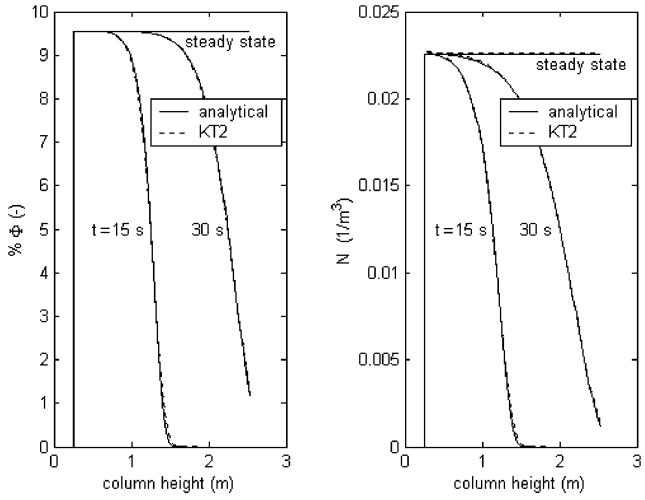

Fig. 6. Comparison between the transient total volume and number concentration profiles and the analytical solution of the PBE (case 1) using the second order discretization scheme with grid dimension: 150×30 for internal and external coordinates, respectively, with $\Delta t = 0.05$ s, $Q_c = 0$ and $Q_d = 1.111 \times 10^{-4}$ m^3/s.

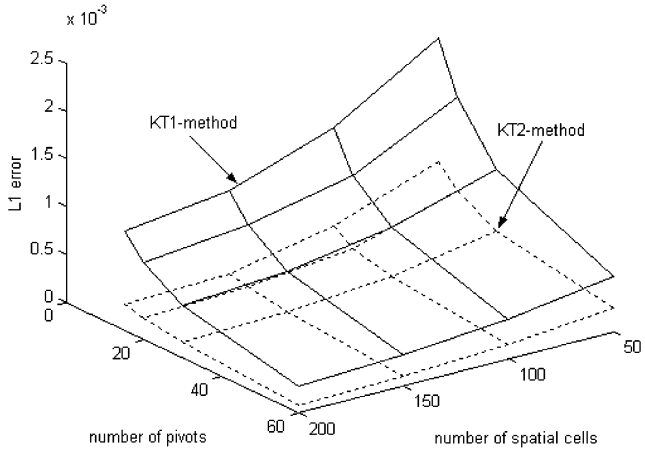

Fig. 7. The convergence characteristics of the first and second order (KT1 & KT2) central differencing schemes using the analytical solution given by Eq. (51) at $t = 10$ s, $\Delta t = 0.05$ s, uniform droplet diameter, nonuniform spatial grids, $Qc = 0.0$ and $Q_d = 1.111 \times 10^{-4}$ m^3/s.

methods are converging in the sense of L1-error ($L_1(t) = \sum_{i=1}^{M_x} \sum_{l=1}^{L} |\varphi_{i,l}^{\langle \text{analyt} \rangle}(t) - \varphi_{i,l}^{\langle \text{num} \rangle}(t)| \Delta d_l \Delta z_i$). The KT2 has an L1-error that is about 40% less than that of KT1. The L1-error for the UW1FVS is the same as that of KT1 and so it is not shown here.

5.2. Case 2: LLEC with droplet breakage and uniform dispersed phase velocity

As it is shown in Appendix A an analytical solution of the PBE given by Eq. (4) is possible in the presence of droplet breakage source term if the dispersed phase velocity considered to have a uniform distribution as it is hypothesized

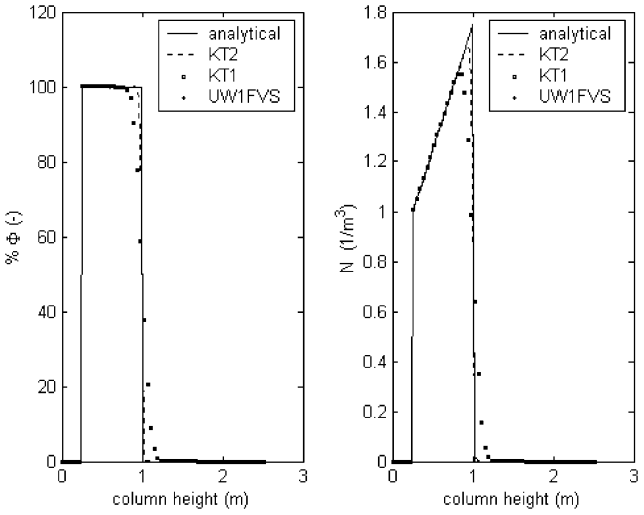

Fig. 8. Comparison between numerical and analytical solutions using the GFP and the spatial discretization schemes for droplet breakage of case 2 on grid with dimension: 300×30, $t = 120$ s, $\Delta t = 0.05$ s, $Q_c = 0$, $Q_d = 1.111 \times 10^{-4}$ m^3/s and $U_d = Q_d/A_c$.

in the classical LLEC models. So, in this case we retain all the assumptions used in case 1 except that $U_d = Q_d/A_c$, $\Gamma = K_b' U_d v(d)$, $\beta_n(d|d') = 6d^2/d'^3$, and $n^{\text{feed}} = N_0^f \, \mathrm{e}^{-\alpha v(d)/v_0}/v_0$ with $N_0^f = 1$, $v_0 = \alpha^2/N_0^f$ to insure feed volume distribution normalization, $K_b' = 1$, and $\alpha = 1$. Based on these simplifications the analytical solution for this case is given by

$$p(d,z,t) = \left(\frac{d}{d_0}\right)^3 \left(\frac{\pi d^2}{2}\right) \left[\frac{\alpha + K_b'(z - z_d)}{\alpha}\right]^2 \times \exp\left[-(\alpha + K_b'(z - z_d))\left(\frac{d}{d_0}\right)^3\right] \times u[t - \tau(d,z)], \tag{54}$$

where the unit step function u is the same as that given by Eqs. (52) and (53) with $U_t = U_d$.

The minimum and maximum droplet diameters are 0.05 and 3.0 mm, respectively, $Q_d = 1.111 \times 10^{-4}$ m^3/s, $\Delta t = 0.05$ s and the final simulation time is 120 s.

In this case the total volume and number concentration profiles have a discontinuity that is moving along the column with a velocity $U_d = Q_d/A_c$. This hypothesized problem is very difficult to solve because of this moving discontinuity and hence it represents a severe test to the spatial discretization schemes as well as the GFP. Fig. 8 shows the analytical and predicted volume and number concentrations using the GFP technique and the UW1FVS, KT1 and KT2 schemes. It is clear that the first order schemes are suffering from some numerical diffusion and need more spatial grid points to reduce it. On the other hand, the second-order scheme has a much better performance near the discontinuities in both volume and number concentrations. In comparison to case 1 we need only 150 spatial cells to almost eliminate the numerical diffusion because the moving front is rather

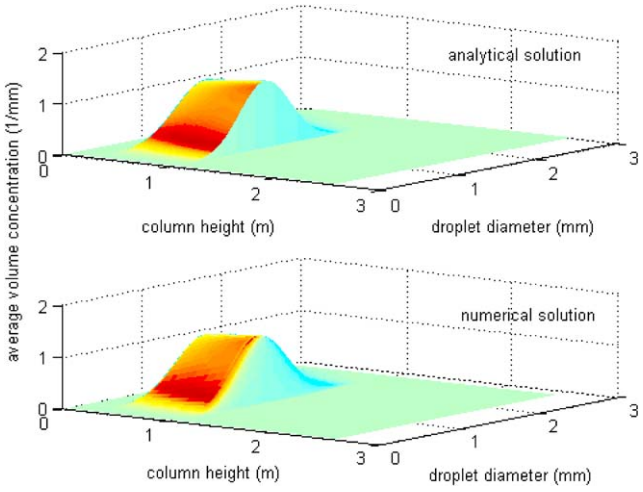

Fig. 9. Comparison of the numerical and exact transient behavior of the average volume concentration using the GFP and the second order central difference scheme (KT2) of case 2 with grid dimensions: 300×30 for internal and external coordinates, respectively, $t = 120$ s, $\Delta t = 0.05$ s, $Q_c = 0$ and $Q_d = 1.111 \times 10^{-4}$ m^3/s.

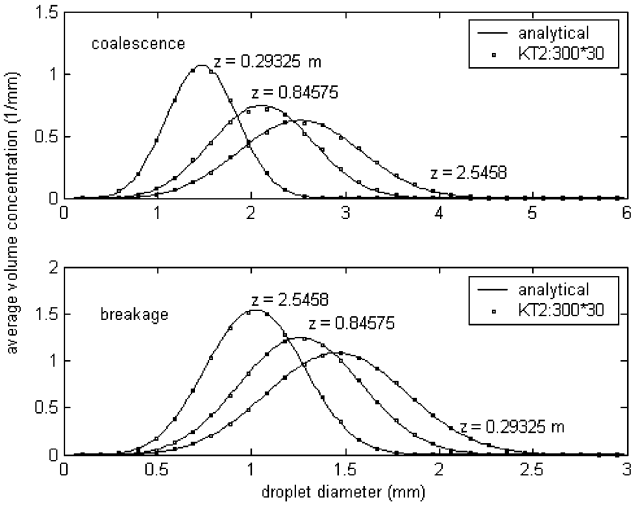

Fig. 10. Steady-state comparison between numerical and analytical solutions using the GFP and the KT2 spatial discretization scheme for droplet breakage (bottom) and coalescence (top) for cases 2 and 3, respectively on grid with dimensions: 300×30, $t = 120$ s, $\Delta t = 2$ s, $Q_c = 0$, $Q_d = 1.111 \times 10^{-4}$ m^3/s, and $U_d = Q_d/A_c$.

more flat than in this case. Moreover, it seems that both droplet breakage and the non-uniform velocity distribution that are responsible for the non-uniform volume concentration profile. This is because when a volume concentration is obtained from the PBE, the source term due to droplet breakage disappears to satisfy the conservation of volume (mass), but this is not the case for the total number concentration. Hence, the total number concentration increases linearly along the column height.

Fig. 9 shows the average volume distribution along the column at $t = 120$ s where the sharp moving front (because of the uniform velocity distribution) seems to be accurately predicted when the analytical (exact) and numerical solutions are compared.

The steady-state convergence of the average volume distribution as compared to the analytical solution at selected positions along the column is shown in Fig. 10, where the steady state is achieved to a tolerance of 10^{-6}.

It is evident that there is a good agreement between the predicted and the analytical solutions, and thus elucidating our trust in the GFP even when the distribution becomes sharp as the column is ascended.

5.3. Case 3: LLEC with droplet coalescence and uniform dispersed phase velocity

This case is devoted to test the presence of droplet coalescence as a source term in the PBE given by Eq. (4). All the assumptions imposed on the PBE in case 2 are applicable here except that the breakage term is set equal to zero. The coalescence frequency is $\omega = K_c U_d$, where $K_c = 1 \times 10^{-9}$ m^2, the minimum and maximum droplet diameters are 0.1 and 5.0 mm, respectively, the final simulation time is $t = 120$ s and $\Delta t = 0.1$ s.

The analytical solution is derived in Appendix A and is given by

$$p(d,z,t) = N_0^f \left(\frac{d}{d_0}\right)^3 \left(\frac{\pi d^2}{2}\right) \left(\frac{2}{2 + N_0^f K_c (z - z_d)}\right)^2 \times \exp\left(\frac{-2(d/d_0)^3}{2 + N_0^f K_c (z - z_d)}\right) u[t - \tau(d,z)], \tag{55}$$

where u is the unit step function given by Eq. (52) with $U_t = U_d$.

Fig. 11 shows the predicted total volume (Φ) and number (N) concentrations using UW1FVS, KT1, and KT2 along with the analytical solution given by Eq. (55). As in case 2, since the dispersed phase velocity distribution is uniform, both these profiles move along the column with a discontinuity having a speed of $U_d = Q_d/A_c$. This makes the numerical solution using the first order schemes more dissipative than the second order one (KT2). Since the total volume of droplet is conserved its concentration profile along the column is uniform; however, the number concentration profile is proportional to the inverse of z, since the droplet coalescence is accompanied by droplet number reduction.

Fig. 10 shows the convergence of the volume distribution as predicted by the KT2 (external coordinate) and the GFP (internal coordinate) schemes at a steady state using grid with dimension: 300×30. It is clear how the volume distribution is shifted to the large droplet size as the dispersed phase ascends the column.

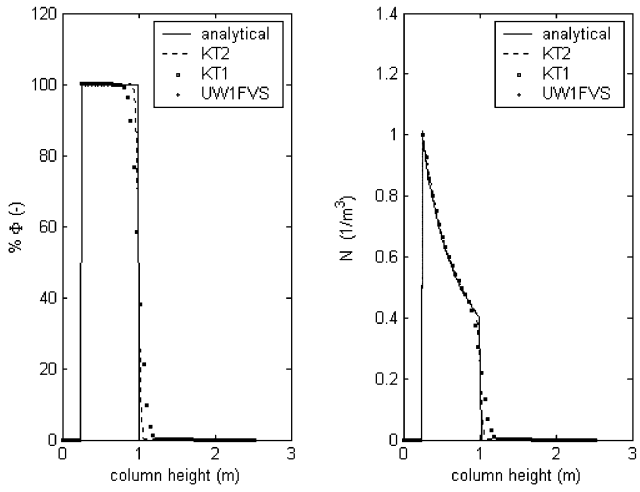

Fig. 11. Comparison between numerical and analytical solutions using the GFP and the spatial discretization schemes for droplet coalescence of case 3 on grid with dimensions: 300×30, $t = 120$ s, $\Delta t = 0.05$ s, $Q_c = 0$, $Q_d = 1.111 \times 10^{-4}$ m^3/s, and $U_d = Q_d/A_c$.

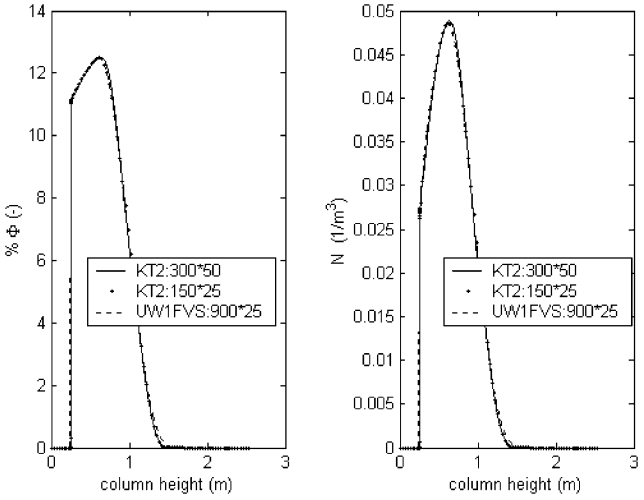

Fig. 12. Convergence of volume and number concentrations using the GFP and the spatial discretization schemes at $t = 15$ s for droplet breakage and coalescence of case 4 with $\Delta t = 0.05$ s, $Q_c = 0.28 \times 10^{-4}$ m^3/s, $Q_d = 1.111 \times 10^{-4}$ m^3/s with uniform droplet diameter and non-uniform spatial grids.

5.4. Case 4: LLEC with droplet breakage and coalescence

In this case we consider a more realistic case including both droplet breakage and coalescence as well as the rigid sphere velocity law given by Eq. (50) with swarm effect function $f = (1 - \phi)$ and slowing factor $K_v = 1$. The feed is given by Weibull distribution with parameters the same as those given in case 1, the breakage frequency is given by $\Gamma = (\pi^2 K_b/36) d^6$ s^{-1} where $K_b = 0.02$ m^{-6}/s, d is in mm and the daughter droplet distribution is the same as that in case 2. The coalescence frequency is given by $\omega = K_c(d^3 + d'^3)$ with $K_c = 0.5$ m^{-6}/s where d is in mm and the dispersion coefficients are $D_c = D_d = 10^{-4}$ m^2/s. The minimum and maximum droplet diameters are 0.25 and 4 mm where breakage and coalescence are active, and 0.25 and 6.5 mm only when droplet coalescence is active. The time step is taken as 0.05 and 2 s for all the transient and steady-state simulations, respectively, with tolerance of 10^{-6} as a criterion for a steady-state approach. Since no analytical solution is available for this case, the numerical convergence is tested through doubling the grid dimensions so that the two consecutive grids produce almost the same solution.

First the discrete models are tested using the non-oscillatory velocity model given in Table 1. Fig. 12 shows the convergence of the GFP and the spatial discretization schemes UW1FVS and KT2 for the prediction of total volume and number concentrations at $t = 15$ s. It is clear that the GFP and the KT2 schemes converge to the solution since the two consecutive grids: 150×25 and 300×50 produced almost the same results. However, the UW1FVS needs a grid of dimension 900×25 to almost converge to the same solution due to its dissipative nature. It should be noted that the moving front in this practical case is not very sharp due to the forward mixing and axial dispersion.

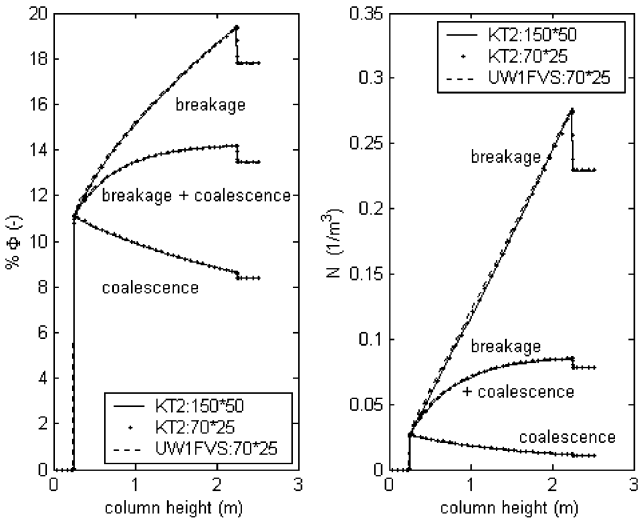

Fig. 13. Steady-state convergence of volume and number concentrations using the GFP and the spatial discretization schemes for droplet breakage and coalescence of case 4 with $\Delta t = 2$ s, $Q_c = 0.28 \times 10^{-4}$ m^3/s, $Q_d = 1.11 \times 10^{-4}$ m^3/s with uniform droplet diameter and non-uniform spatial grids.

Fig. 13 shows the steady-state convergence of the GFP and the spatial discretization schemes in the presence of different droplet interaction mechanisms. The KT1 scheme is found to produce identical results as UW1FVS and hence it is not shown here. First the solution is converging for different droplet interactions on consecutive grids: 70×25 and 150×50 for both total volume and number concentrations, indicating that the first-order schemes are accurate enough to predict the hydrodynamic behavior of LLECs at a steady state. Second, the discrete model behavior seems to correctly

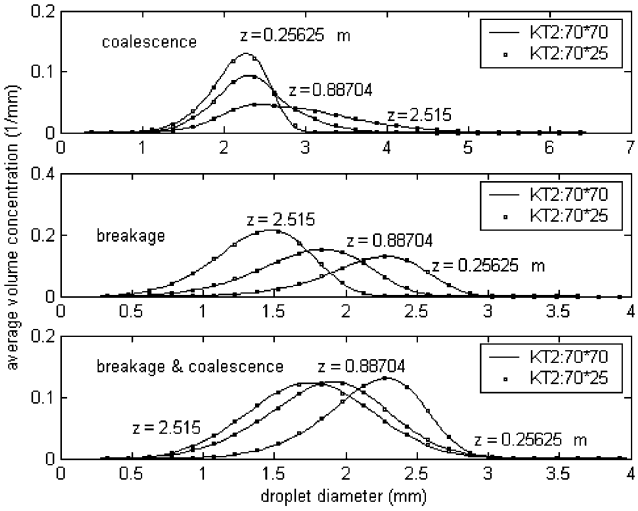

Fig. 14. Steady-state convergence of the average volume distributions along the column using the GFP and the KT2 spatial schemes for droplet breakage and coalescence of case 4 with $\Delta t = 2$ s, $Q_c = 0.28 \times 10^{-4}$ m^3/s, $Q_d = 1.11 \times 10^{-4}$ m^3/s with uniform droplet diameter and non-uniform spatial grids.

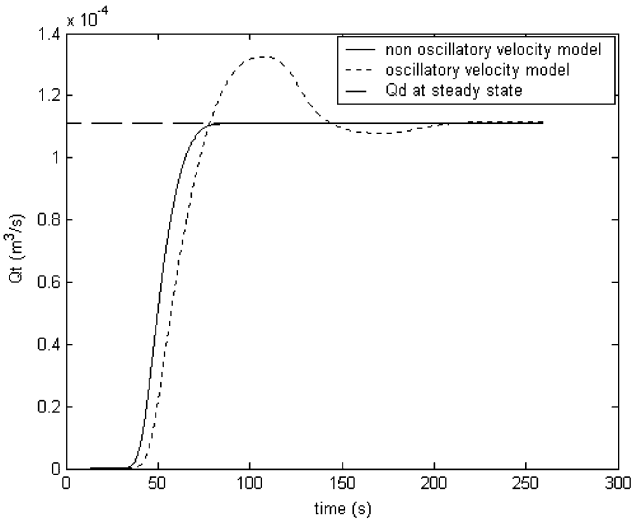

Fig. 15. Comparison between the oscillatory and non-oscillatory velocity models using KT2 scheme for droplet breakage and coalescence of case 4 with $\Delta t = 0.1$ s, $Q_c = 0.28 \times 10^{-4}$ m^3/s, $Q_d = 1.11 \times 10^{-4}$ m^3/s using uniform droplet diameter and non-uniform spatial grids of dimension 150×30.

Table 3
The steady-state convergence of the GFP and the spatial discretization schemes based on case 4 with nonuniform and uniform spatial and droplet diameter grids, respectively

$L \times M_x$	Systematic error			CPU[a] time (s)		
	FVS	KT1	KT2	FVS	KT1	KT2
50×15	0.00611	0.00062	0.00091	5	5	6
100×30	0.00171	0.00038	0.00016	28	29	31
150×45	0.00065	0.00032	0.00013	148	156	159

[a]The CPU times were estimated under Compaq visual FORTRAN version 6.6 environment using a PC Pentium III 750 MHz processor.

reflect the different droplet interactions in the column. For droplet breakage alone the volume and number concentration profiles change sharply along the column height. This is because as the droplets ascend the column the droplets break up and hence their rise velocity is reduced resulting in an increased total volume and number concentrations. The reverse situation is true when only droplet coalescence is active. Since in reality, both droplet breakage and coalescence are active, we expect the volume and number concentrations profiles to lie within the limits of the two previous cases as shown in Fig. 13 which is observed experimentally in Kühni (Gerstlauer, 1999) and RDC columns (Modes, 2000).

Fig. 14 shows the convergence of the GFP technique at fixed spatial grid using the KT2 scheme for spatial discretization. It is clear that the GFP technique is converging on consecutive grids: 70×25 and 70×70 for various droplet interaction mechanisms along the column. Table 3 sheds more light on the quantitative convergence characteristics of the internal and external discretization schemes as well as the CPU time requirements. The convergence test is based on the mean droplet diameter $\overline{d30}$ with respect to diameter and column height. Since no analytical solution is available, we used a reference solution on grid whose dimension is 300×60 at a steady state. It is clear that the discretization in both dimensions is converging with small systematic errors, where the KT2 scheme is the most accurate one. It is also interesting to note that the CPU time requirements for the second-order scheme KT2 using 500 integration steps is almost the same as that of the first-order schemes: KT1 and UW1FVS with the gain of higher accuracy.

To see the difference between the conventional and the improved velocity models given by Eq. (13) and Table 1, we simulate these two models using the parameters of this case. Fig. 15 shows the response of the dispersed phase flow rate at the top of the column using oscillatory and non-oscillatory velocity models. It is clear how the improved velocity model completely eliminates the oscillation behavior of the dispersed phase by simply manipulating the inlet continuous phase flow rate. This oscillatory behavior, due to manipulating the continuous flow rare at the bottom of the column (Fig. 1), is observed experimentally by many authors and the interested reader could refer to Hufnagl et al. (1991), Weinstein et al. (1998) and Gerstlauer (1999).

6. Experimental validation

In order to get more trust in the present population balance model and its discrete counterparts, we compare its predictions to some of the available experimental work in the published literature. From this, is the recent experimental data of Modes (2000) for the steady-state hydrodynamics of a laboratory scale RDC column whose dimensions

Table 4
Droplet breakage and transport functions as correlated by Modes (2000)

Slowing factor	Axial dispersion coefficient (dispersed phase)
$K_v(d,N^*)=1-1.037(N^{*3}D_R^5)^{0.12}-0.62\left(\frac{d}{D_s-D_R}\right)^{0.44}$	$\frac{D_d}{U_dH}=0.0138+8.26\times10^{-7}\left(\frac{N^*D_R}{U_d}\right)^{3.3}$
Droplet breakage probability	**Daughter droplet distribution**
$\frac{P_r}{1-P_r}=6.04\times10^{-4}\left(\frac{\rho_c^{0.8}\mu_c^{0.2}dD_R^{1.6}(\omega_R^{1.8}-\omega_{R,\mathrm{crit}}^{1.8})}{\sigma}\right)^{1.595}$	$\beta_n(d\|d')=3\vartheta(\vartheta-1)\left[1-\left(\frac{d}{d'}\right)^3\right]^{(\vartheta-2)}\frac{d^2}{d'^3}$

are shown in Table 2. The experimentally correlated droplet transport functions, the breakage frequency, and the daughter droplet distribution are used for model validation. These were determined based on single droplet experiments carried out in a column segment having five compartments of total height of 0.15 m. The droplet rise velocity and the breakage probability functions are determined using digital image processing, while the axial dispersion coefficient of the dispersed phase is determined using residence time analysis for a monodispersion of droplets of specified diameters (Modes et al., 1999). Due to the relative high interfacial tension of the used chemical system (water-toluene), the low values of dispersed phase hold-up, and in the absence of mass transfer, the droplet coalescence could be safely neglected. Additionally, Modes (2000) recommended the use of Vignes (1965) velocity law to estimate the terminal droplet velocity multiplied by $(1-\phi)$ to take into account the droplet swarm effect (see Eq. (10)). This author correlated the slowing factor, K_v, and the axial dispersion coefficient, D_d, with the energy input and the droplet diameter as shown in Table 4, where N^* is the rotor speed (s^{-1}), and the dimensions of the rotor (D_R) and stator (D_s) diameters are shown in Table 2.

The droplet breakage frequency is expressed in terms of the droplet residence time and the breakage probability and is given by

$$\Gamma(d,\phi)=P_r(d,N^*)\,\frac{U_d(d,\phi)}{H_c}. \tag{56}$$

The breakage probability, P_r, is correlated with the system physical properties, the energy dissipation as shown in Table 4. The critical rotor speed, $\omega_{R,\mathrm{crit}}$, is introduced to take into account the population of droplets whose breakage probability falls to zero. This is because the shear force imparted to the droplets by the rotor blade is not enough to exceed the droplet surface energy (Modes, 2000). The daughter droplet distribution (based on number), as shown in Table 4, is assumed to follow the beta distribution, where ϑ is the mean number of daughter droplets produced upon breakage of mother droplet of diameter d'. It is experimentally correlated and found dependent on the energy dissipation and having a value $\geqslant 2$. Note that when ϑ is equal 2 the above daughter droplet distribution is reduced to the uniform distribution with respect to droplet volume as internal coordinate.

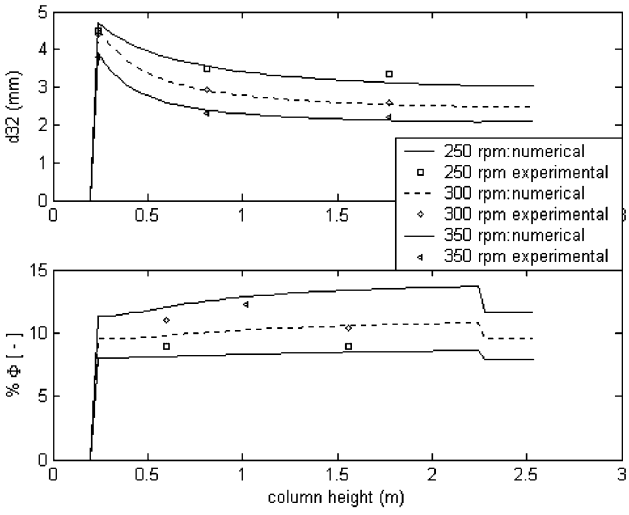

Fig. 16. Steady-state comparison between the experimental data and the model prediction with two energy inputs using grid dimension: 70×20 and $Q_c=2.78\times10^{-5}$, $Q_d=3.33\times10^{-5}$ m^3/s. The experimental data are from Modes (2000).

In all the numerical simulations presented in this section the inlet feed distribution is based on the measured values and for the convergence tests the log normal distribution is fitted to the experimental data. The integration is carried out until a steady state with a time step $\Delta t=2$ s. The UW1FVS discrete model with uniform grid, having a dimension of 70×20, is used for spatial discretization, where doubling of the grid size shows no principal differences in the predicted results. The minimum droplet diameter is chosen to lie below the critical droplet diameter, and the maximum droplet size is estimated based on the initial and feed droplet distributions such that Eq. (28) is satisfied.

Fig. 16 compares the predicted mean droplet diameter, d32, and the dispersed phase hold-up at three rotor speeds, 250, 300 and 350 rpm. The predicted and experimental values of the mean droplet diameter seems to be in good agreement with the experimental data, however, the predicted hold-up values are not as good as the predicted d32. This is because the errors in the volume distribution seem to cancel when the d32 is calculated since it involves the ratio of droplet volume to its surface area. Nevertheless, the model

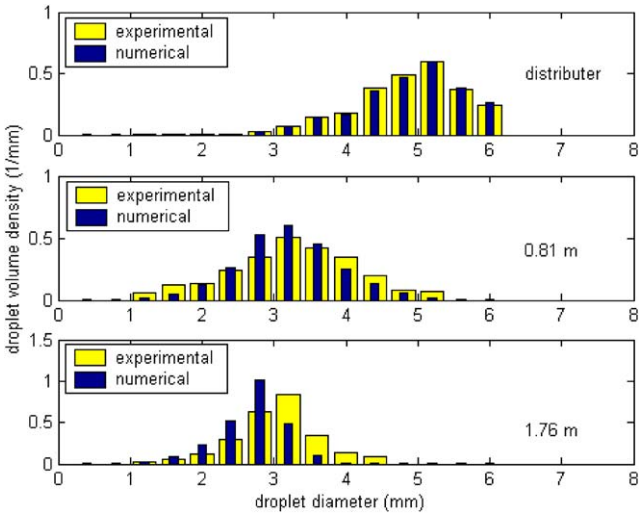

Fig. 17. Steady-state comparison between experimental data and the model prediction at 300 rpm using grid dimension: 70×20, $Q_c=1.39\times10^{-5}$ and $Q_d=3.33\times10^{-5}$ m^3/s. The experimental data are from Modes (2000).

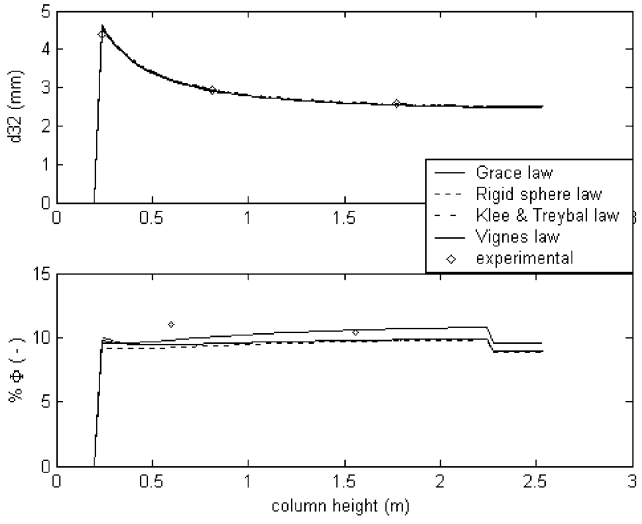

Fig. 18. The effect of the different velocity models (Grace et al., 1976; Klee and Treybal, 1956; Vignes, 1965) on the steady-state d32 and the total column hold-up with grid dimensions: 70×20, $Q_c=2.78\times10^{-5}$ and $Q_d=3.33\times10^{-5}$ m^3/s. The experimental data are from Modes (2000).

correctly follows the experimental trend where the hold-up increases as the rotor speed increases, indicating an increase in the droplet breakage.

Fig. 17 shows the predicted and experimental droplet volume densities at rotor speed 300 rpm corresponding to the measuring points along the column. The model predicts fairly well the volume distribution along the column; however, the error increases as the droplet is shifted to the left indicating the breakage of the droplets as they ascend the column.

In Fig. 18, we examined the effect of different droplet terminal velocity laws on the predicted mean droplet diameter and the dispersed phase hold-up. Again, it seems that the error cancellation, when calculating the mean droplet diameter, makes it less sensitive to the type of the velocity law than the dispersed phase hold-up. Anyhow, we need more experimental hold-up data to select the right terminal velocity law that well describe the chemical system under investigation. Note that the sensitivity analysis of the model predictions with respect to certain parameters such as, K_v, D_d, Γ, and ϑ is not considered in this work since this issue is analyzed by (Modes, 2000). He found that the greatest model sensitivity is with respect to the droplet-slowing factor, K_v. It should also be pointed out that the model predicts the flooding behavior of the column when an excessive entrainment of the dispersed phase is observed at the bottom of the column. However, further flooding analysis can be found in Gourdon and Casamatta (1994) and will not be detailed here.

7. Conclusions

The comprehensive literature review of the available numerical techniques showed that the zero-order methods which are inherently consistent, with respect to specific droplet integral properties posses the simplicity, robustness, and accuracy for solving the general PBEs. Among these methods, the fixed-pivot technique of Kumar and Ramkrishna (1996a), is the best candidate for this task. So, in this work we generalized the fixed-pivot technique to solve the general PBE for continuous flow systems showing both internal and external coordinates dependency. The external coordinate discretization is carried out using simplified upwind and central differencing schemes, where the latter have the advantage of being free of any approximate Riemann solvers. The combined internal and external discretization schemes are found very efficient in solving extremely difficult cases for typical LLECs including droplet breakage and coalescence. The discrete models are validated using four cases, of which three have known analytical solutions that are derived in this work. In all these case studies the discretization schemes were able to predict the analytical solutions and found convergent to solutions on fine grids where the analytical solutions are not available. The second-order central differencing scheme (KT2) is found the most accurate to capture the moving profiles along the column; however, the three differencing schemes have almost the same accuracy for steady-state simulations if sharp profiles are not likely to appear. Moreover, the CPU time requirement for the second-order scheme was found comparable to the first-order ones with a remarkable high accuracy.

The transient behavior of the dispersed phase hold-up is found dependent on the type of the continuous phase velocity model. In this work, we derived a continuous phase velocity model that is non-oscillatory based on the idea of Hufnagl et al. (1991), and hence it is superior to

the oscillatory model derived by Casamatta (1981). The comparison of the upwind first order central differencing scheme with the experimental data at steady state was found very satisfactory. The model is found to well predict the general LLEC hydrodynamic behavior at different rotor speeds. So, it is concluded that the combination of the GFP and UW1FVS provides a powerful and robust solver for the PBE describing the hydrodynamic behavior of general LLECs. Due to this we are currently extending these schemes to the more general case when mass transfer is included.

Notation

$\boldsymbol{A}$	breakage interaction matrix, Eq. (25)
A_c	column cross-sectional area
$\boldsymbol{d}$	characteristic droplet diameter vector
d, d'	droplet diameter, mm
d_0	mean droplet diameter of the initial or feed droplet distribution, mm
d_i, $d_{i+1/2}$	the characteristic droplet diameter and the right boundary of the ith subdomain respectively, mm
$d_{\min}$, $d_{\max}$	minimum and maximum droplet diameters, mm
d30, d32	mean droplet diameters, mm
$\overline{\text{d30}}$	mean droplet diameter with respect to d and column height, mm
D_c, D_d	diffusion coefficients for the continuous and dispersed phases, respectively, m^2/s
D_R, D_s	rotor and stator diameters, respectively, m
f^{feed}	inlet feed distribution, m^{-1}
F	the convective flux: $U_d n$ or $U_d p$, s^{-1} m^{-3} or s^{-1}
FDE^L, FDE^U	average lower and upper finite domain errors, Eq. (28)
g	the acceleration of gravity, m s^2
H, H_c	column and single compartment heights, respectively, m
I_i	integral quantity based on the property $u_m(d_i)$ in the ith subdomain
$\overline{I_i}$	average integral quantity based on the property $u_m(d_i)$ in the ith subdomain, Eq. (47)
K_b, K_c	breakage and coalescence frequency constants
L	number of external (spatial) coordinate cells
M_x	number of subdomain of the internal coordinate (pivots)
n	number distribution function, m^{-4}
n_0, n^{ic}	initial number distribution function, m^{-1}
n^{feed}	feed number distribution function, m^{-1}
N_0^f	number concentration in the inlet feed, m^{-3}
N_i	droplet number concentration in the ith subdomain, mm^{-3}
N^*	rotor speed, s^{-1}
p	volume distribution function, m^{-1}
$\boldsymbol{P}$	physical properties vector
P_r	breakage probability, Table 4
Q_b	dispersed phase flow rate at bottom of the column, m^3/s
Q_d	dispersed phase flow rate, m^3/s
Q_c,	continuous phase flow rate, m^3/s
Q_t	dispersed phase flow rate at top of the column, m^3/s
$\boldsymbol{r}$	external coordinate victor: $[x, y, z]$
r	spectral radius of the Jacobian matrix
$\boldsymbol{S}$	local propagation speed, Eq. (45)
$SysErr$	systematic error, Eq. (48)
t	time, s
u_m	any property associated with single droplet
U_c	continuous phase velocity relative to the column walls, m/s
U_d	dispersed phase velocity relative to the column walls, m/s
U_r	relative droplet (slip) velocity, m/s
U_t	terminal droplet velocity, m/s
v, v'	droplet volumes, m^3
v_0, v_f	mean droplet volume of the initial condition and feed distributions, m^3
$v_{\min}$, $v_{\max}$	minimum and maximum droplet volume, m^3
x_i	the characteristic droplet volume in the ith subdomain, m^3
z	spatial coordinate, m
z_c	continuous phase inlet, m
z_d	dispersed feed inlet, m

Greek letters

α	parameter in the Weibull and inlet feed distributions
α_c, α_d	as defined in Table 1
β	parameter in the Weibull distribution
β_n	daughter droplet distribution based on droplet number, mm^{-1}
$\gamma_i^{\langle i-1\rangle}$, $\gamma_i^{\langle i\rangle}$	linear functions satisfying Eq. (17)
Γ	droplet breakage frequency, s^{-1}
ζ	as defined by Eq. (27)
θ	TVD parameter between 1 and 2.
μ_c	continuous phase viscosity, kg/m/s
ρ, $\rho_{b,i}$, $\rho_{c,i}$	breakage and coalescence source terms, Eqs. (2), (21), and (24)
ρ_c, ρ_d	density of the continuous and dispersed phases respectively, kg/m^3
σ	interfacial tension, N/m^{-1}
τ	residence time, s
ϕ, Φ	total dispersed phase hold-up
ϕ_e	dispersed phase hold-up entrained with the continuous phase
φ_i	dispersed phase hold-up in the ith subdomain

$\Psi^{\langle i \rangle}$	the ith coalescence interaction matrix, Eq. (22)
ω	droplet coalescence frequency, m^3/s^{-1}
ω_R, $\omega_{R,\mathrm{crit}}$	rotor and critical rotor speeds respectively, s^{-1}
$\vartheta(v')$	average number of droplets produced when mother droplet of volume, v', is broken

Acknowledgements

The authors wish to thank the DFG (Deutsche Forschungsgemeinschaft) and DAAD (Deutscher Akademischer Austauschdienst) for supporting this work.

Appendix A. Analytical solution of the simplified PBE

To the best of the author's knowledge there is no analytical solution to the general PBE given by Eq. (4). However, Campos and Lage (2003) tried to solve it for droplet breakage and growth using the successive generation method of Liou et al. (1997) by neglecting the diffusion term and assuming constant U_d. Unfortunately, they were not able to obtain an analytical solution in the closed from, and hence their semi-analytical solution requires further sophisticated programming as they pointed out. In this section we present an efficient methodology for solving the PBE with uniform dispersed phase velocity in a stagnant continuous phase, negligible diffusion flux and zero initial condition. So, let us simplify Eq. (4) based on these assumptions to get

$$\frac{\partial n}{\partial t} + U_d \frac{\partial n}{\partial \zeta} = \rho\{n, v\}, \tag{A.1}$$

where $\zeta = z - z_d.$, $U_d = Q_d/A_c$ and the boundary condition is given by

$$n(v, 0, t) = \frac{Q_d}{A_c} n^{\mathrm{feed}} \quad \text{at } \zeta = 0. \tag{A.2}$$

Due to the convective nature of Eq. (A.1) with uniform droplet velocity, it is well known that the response of the dispersed phase cannot occur until the local residence time, ζ/U_d is exceeded. So, let us define the relative time, η as

$$\eta(t, \zeta) = t - \frac{\zeta}{U_d}. \tag{A.3}$$

Now making the necessary variable transformation using the chain rule, Eq. (A.1) could be reduced to

$$U_d \frac{\partial n(v; \eta, \zeta)}{\partial \zeta} = \rho\{n(v; \eta, \zeta), v\} \tag{A.4}$$

with the following boundary condition:

$$n(v, 0, \eta) = \frac{Q_d}{A_c} n^{\mathrm{feed}} \quad \text{at } \zeta = 0 \text{ and } \eta > 0. \tag{A.5}$$

Note that we can treat the spatial variable ζ as a like time variable and hence the first order IPDE given by Eqs. (A.4) and (A.5) could be solved in the same way as we solve the PBE for a batch stirred tank. It is then this important analogy between Eq. (A.4) and the batch PBE that makes our approach very general and effective in obtaining an analytical solution whenever it is possible to solve the batch PBE. For example, all the analytical solutions reported by Gelbard and Seinfeld (1978) are valid solutions to Eqs. (A.4) and (A.5) by simply replacing the time variable in it by ζ. Following this methodology, we can derive the analytical solutions for case 2 (Eq. (56)) by simply using the analytical solution for droplet breakage in a batch stirred tank that is given by Ziff and McGrady (1985) after transforming it in terms of droplet diameter:

$$n(d, \zeta, \eta) = \left(\frac{\pi d^2}{2}\right) \left[\frac{\alpha + K_b' \zeta}{\alpha}\right]^2 \times \exp\left[-(\alpha + K_b' \zeta)\left(\frac{d}{d_0}\right)^3\right] u[\eta]. \tag{A.6}$$

Note that the unit step function, u, is used since $\eta \geqslant 0$ and the part of the column in front of the moving dispersed phase is completely empty because of the zero initial condition. Now rewriting this equation in terms of the original variables and the volume distribution p we get

$$p(d, z, t) = \left(\frac{d}{d_0}\right)^3 \left(\frac{\pi d^2}{2}\right) \left[\frac{\alpha + K_b'(z - z_d)}{\alpha}\right]^2 \times \exp\left[-(\alpha + K_b'(z - z_d))\left(\frac{d}{d_0}\right)^3\right] \times u[t - \tau(d, z)]. \tag{A.7}$$

This is exactly the same as Eq. (56) and the unit step function is defined by Eqs. (55) and (55).

Similarly, Eq. (55) is derived by using the analytical solution for droplet coalescence in batch stirred tank as reported by Gelbard and Seinfeld (1978) after transforming it in terms of droplet diameter:

$$n(d, \zeta, \eta) = N_0^f \left(\frac{\pi d^2}{2}\right) \left(\frac{2}{2 + N_0^f K_c \zeta}\right)^2 \times \exp\left(\frac{-2(d/d_0)^3}{2 + N_0^f K_c \zeta}\right) u[\eta]. \tag{A.8}$$

By substituting η and ζ in the above equation and rewriting it in terms of volume distribution p we recover exactly Eq. (55).

It should be pointed out that the droplet growth could be included in Eq. (A.1) in a straightforward manner, and hence we could also get solutions for Eq. (A.1), whenever this is possible in batch stirred tank.

Appendix B. Estimation of the total finite domain error (FDE)

Let us start from the average lower and upper FDEs as given by (Attarakih et al., 2003a):

$$\mathrm{FDE} = \frac{1}{\Delta d}\sum_{m=1}^{2}\int_{0}^{d_{\min}} u_m(d)n(d;z,t)\delta d + \lim_{d\to\infty}\frac{1}{\Delta d}\int_{d_{\max}}^{d} u_m(d)n(d;z,t)\partial d = \sum_{m=1}^{2}(\mathrm{FDE}_m^L + \mathrm{FDE}_m^U). \tag{B.1}$$

In breakage and coalescence process, the minimum and maximum droplet sizes could be initially estimated based on the inlet feed and initial condition distributions such that $\mathrm{FDE}_m^U < \mathrm{TOL}/2$ $(m = 1, 2)$, where TOL is a real and small positive number. These upper and lower residuals could be fairly approximated using the available values of the discrete distributions (the first and last two discrete values will be used) so that Eq. (B.1) could be written as

$$\mathrm{FDE}^L = \sum_{m=1}^{2}\sum_{i=1}^{2}\frac{1}{\Delta d_i}u_m(d_i)N_i(z,t) + \frac{1}{\Delta d}\sum_{m=1}^{2}\int_{0}^{d_{\min}} u_m(d)n(d;z,t)\partial d, \tag{B.2}$$

$$\mathrm{FDE}^U = \sum_{m=1}^{2}\sum_{i=M_x-1}^{M_x}\frac{1}{\Delta d_i}u_m(d_i)N_i(z,t) + \lim_{d\to\infty}\frac{1}{\Delta d}\sum_{m=1}^{2}\int_{d_{\max}}^{d} u_m(d)n(d;z,t)\partial d. \tag{B.3}$$

Note that

$$\sum_{m=1}^{2}\sum_{i=1}^{2}\frac{1}{\Delta d_i}\int_{d_{i-1/2}}^{d_{i+1/2}} u_m(d)n(d;z,t)\partial d > \frac{1}{\Delta d}\sum_{m=1}^{2}\int_{0}^{d_{\min}} u_m(d)n(d;z,t)\partial d \tag{B.4}$$

since the number distribution function should be monotone increasing at least for $d \in [0, d_{\min} + 2\Delta d]$ because of the lower boundary condition. This makes the following condition always valid:

$$\sum_{m=1}^{2}\sum_{i=1}^{2}\frac{1}{\Delta d_i}\int_{d_{i-1/2}}^{d_{i+1/2}} u_m(d)n(d;z,t)\partial d \leqslant \mathrm{TOL}/2 \Rightarrow \frac{1}{\Delta d}\sum_{m=1}^{2}\int_{0}^{d_{\min}} u_m(d)n(d;z,t)\partial d < \mathrm{TOL}/2. \tag{B.5}$$

Similarly

$$\sum_{m=1}^{2}\sum_{i=M_x-1}^{M_x}\frac{1}{\Delta d_i}\int_{d_{i-1/2}}^{d_{i+1/2}} u_m(d)n(d;z,t)\partial d > \lim_{d\to\infty}\frac{1}{\Delta d}\sum_{m=1}^{2}\int_{d_{\max}}^{d} u_m(d)n(d;z,t)\partial d. \tag{B.6}$$

Since the number distribution function should be monotone decreasing at least for $d \in [d_{\max} - 2\Delta d, d_{\max},]$ because of the upper boundary condition, it follows that

$$\sum_{m=1}^{2}\sum_{i=M_x-1}^{M_x}\frac{1}{\Delta d_i}\int_{d_{i-1/2}}^{d_{i+1/2}} u_m(d)n(d;z,t)\partial d \leqslant \mathrm{TOL}/2 \Rightarrow \lim_{d\to\infty}\frac{1}{\Delta d}\sum_{m=1}^{2}\int_{d_{\max}}^{d} u_m(d)n(d;z,t)\partial d < \mathrm{TOL}/2 \tag{B.7}$$

and hence $d_{\min}$ and $d_{\max}$ could be safely estimated at fixed M_x and TOL from the following relation:

$$\mathrm{FDE}(d_{\min}, d_{\max}, M_x) = \mathrm{FDE}^L + \mathrm{FDE}^U \leqslant \mathrm{TOL}, \tag{B.8}$$

where

$$\mathrm{FDE}^L \approx \sum_{m=1}^{2}\sum_{i=1}^{2}\frac{1}{\Delta d_i}u_m(d_i)N_i(z,t) + \sum_{m=1}^{2}\sum_{i}^{2}\frac{1}{\Delta d_i}\times\left(\int_{d_{i-1/2}}^{d_{i+1/2}} u_m(d)n^{\mathrm{feed}}(d)\partial d + \int_{d_{i-1/2}}^{d_{i+1/2}} u_m(d)n^{ic}(d)\partial d\right), \tag{B.9}$$

$$\mathrm{FDE}^U \approx \sum_{m=1}^{2}\sum_{i=M_x-1}^{M_x}\frac{1}{\Delta d_i}u_m(d_i)N_i(z,t) + \sum_{m=1}^{2}\sum_{i=M_x-1}^{M_x}\frac{1}{\Delta d_i}\times\left(\int_{d_{i-1/2}}^{d_{i+1/2}} u_m(d)n^{\mathrm{feed}}(d)\partial d + \int_{d_{i-1/2}}^{d_{i+1/2}} u_m(d)n^{ic}(d)\partial d\right) \tag{B.10}$$

which are the required relations given by Eqs. (30)–(32).

References

Alatiqi, I., Aly, G., Mjalli, F., Mumford, C.J., 1995. Mathematical modeling and steady-state analysis of a Scheibel extraction column. Canadian Journal of Chemical Engineering 73, 523–533.

Al Khani, S.D., Gourdon, C., Casamatta, G., 1988. Simulation of hydrodynamics and mass transfer of disks and rings pulsed column. Industrial and Engineering Chemistry Research 27, 329–333.

Al Khani, S.D., Gourdon, C., Casamatta, G., 1989. Dynamic and steady-state simulation of hydrodynamics and mass transfer in liquid–liquid extraction column. Chemical Engineering Science 44, 1295–1305.

Alopaeus, V., Koskinen, J., Keskinen, K.I., Majander, J., 2002. Simulation of the population balances for liquid–liquid systems in a nonideal stirred tank: part 2—parameter fitting and the use of multiblock model for dense dispersions. Chemical Engineering Science 57, 1815–1825.

Attarakih, M.M., Bart, H.J., Faqir, N.M., 2003a. Optimal moving and fixed grids for the solution of discretized population balances in batch and continuous systems: droplet breakage. Chemical Engineering Science 58, 1251–1269.

Attarakih, M.M., Bart, H.-J., Faqir, N.M., 2003b. Solution of the population balance equation for liquid–liquid extraction columns using a generalized fixed-pivot and central difference schemes. In: Kraslawski, A., Turunen, I. (Eds.), European Symposium on Computer Aided Process Engineering-13, Computer-Aided Chemical Engineering, Vol. 14. Elsevier, Amsterdam, pp. 557–562.

Attarakih, M.M., Bart, H.J., Faqir, N.M., 2004. Solution of the droplet breakage equation for interacting liquid–liquid dispersions: a conservative discretization approach. Chemical Engineering Science, this issue (doi: 10.1016/j.ces.2004.03.004).

Bart, H.-J., 2003. Reactive extraction in stirred columns: a review. Chemical Engineering and Technology 26, 723–731.

Bennett, M.K., Rohani, S., 2001. Solution of population balance equations with a new combined Lax–Wendroff/Crank–Nicholson method. Chemical Engineering Science 56, 6623–6633.

Biggs, C.A., Lant, P.A., 2002. Modelling activated sludge flocculation using population balances. Powder Technology 14, 201–211.

Cabassud, M., Gourdon, C., Casamatta, G., 1990. Single drop break-up in a Kühni column. Chemical Engineering Journal 44, 27–41.

Campos, F.B., Lage, P.L.C., 2003. A numerical method for solving the transient multidimensional population balance equation using Euler–Lagrange formulation. Chemical Engineering Science 58, 2725–2744.

Casamatta, G., 1981. Comportement de la population des gouttes dans une colonne d'extraction: transport, rupture, coalescence, transfer de matiere, Dissertation, Institut National Polytechnique De Toulouse.

Casamatta, G., Vogelpohl, A., 1985. Modelling of fluid dynamics and mass transfer in extraction columns. German Chemical Engineering 8, 96–103.

Cauwenberg, V., Degreve, J., Slater, M.J., 1997. The interaction of solute transfer, contaminants and drop break-up in rotating disc contactors: part I. Correlation of drop breakage probabilities. Canadian Journal of Chemical Engineering 75, 1046–1055.

Chang, S.-C., Wang, X.-Y., Chow, C.-Y., 1999. The space-time conservation element and solution element method. A new high-resolution and genuinely multidimensional paradigm for solving conservation laws. Journal of Computational Physics 156, 89–136.

Chatzi, E., Lee, J.M., 1987. Analysis of interactions for liquid–liquid dispersions in agitated vessels. Industrial and Engineering Chemistry Research 26, 2263–2267.

Colella, D., Vinci, D., Bagatin, R., Masi, M., 1999. A study on coalescence and breakage mechanisms in three different bubble columns. Chemical Engineering Science 54, 4767–4777.

Coulaloglou, C.A., Tavlarides, L.L., 1977. Description of interaction processes in agitated liquid–liquid dispersions. Chemical Engineering Science 32, 1289–1297.

Desnoyer, C., Masbernat, O., Gourdon, C., 2003. Experimental study of drop size distribution at high phase ratio in liquid–liquid dispersions. Chemical Engineering Science 58, 1353–1363.

Diemer, R.B., Olson, J.H., 2002a. A moment methodology for coagulation and breakage problems: part 1—analytical solution of the steady-state population balance. Chemical Engineering Science 57, 2193–2209.

Diemer, R.B., Olson, J.H., 2002b. A moment methodology for the coagulation and breakage problems: part 2—moment models and distribution reconstruction. Chemical Engineering Science 57, 2211–2228.

Gelbard, F., Seinfeld, J.H., 1978. Numerical solution of the dynamic equation for particulate systems. Journal of Computational Physics 28, 357–375.

Gelbard, F., Tambour, Y., Seinfeld, J.H., 1980. Sectional representation of simulating aerosol dynamics. Journal of Colloid & Interface Science 76, 541–556.

Gerstlauer, A., 1999. Herleitung und Reduktion populationsdynamischer Modelle am Beispiel der Fluessig-Fluessig-Extraktion. Fortschritt-Berichte VDI Reihe 3, 612.

Godfrey, J.C., Slater, M.J., 1991. Slip velocity relationships for liquid–liquid extraction columns. Transactions of the Institution of Chemical Engineers 69, 130–141.

Goodson, M., Kraft, M., 2003. Stochastic simulation of coalescence and breakage processes: a practical study. Preprint No. 9, Cambridge Center for Computational Chemical Engineering, Cambridge, pp. 1–30.

Gourdon, C., Casamatta, G., 1994. Population balance based modeling of solvent extraction columns. Liquid–Liquid Extraction Equipment. Wiley, New York, pp. 136–226.

Grace, J.R., Wairegi, T., Nguyen, T.H., 1976. Shapes and velocities of single drops and bubbles moving freely through immiscible liquids. Transactions of the Institutiton of Chemical Engineers 54, 167–173.

Guimaraes, M.M., Cruz-Pinto, J.J.C., Regueiras, P.F.R., Madureira, C.M.N., 1992. The simulation of interacting liquid–liquid dispersions—a new algorithm and its potentiality. In: Sekine, T. (Ed.), Solvent Extraction 1990, Part B. Elsevier, Amsterdam, pp. 1241–1246.

Hamilton, R.A., Curits, J.S., Ramkrishna, D., 2003. Beyond log-normal distributions: Hermite spectra for solving population balances. A.I.Ch.E. Journal 49, 2328–2343.

Hartland, S., Jeelani, S.A.K., 1994. Gravity settlers. In: Godfrey, J.C., Slater, M.J. (Eds.), Liquid–liquid Extraction Equipment. Wiley, New York.

Hill, P.J., Ng, K.M., 1995. New discretization procedure for the breakage equation. A.I.Ch.E. Journal 41, 1204–1216.

Hill, P.J., Ng, K.M., 1996. New discretization procedure for the agglomeration equation. A.I.Ch.E. Journal 42, 727–741.

Hill, P.J., Ng, K.M., 1997. Simulation of solids processes accounting for particle-size distribution. A.I.Ch.E. Journal 43, 715–726.

Hounslow, M.J., 1990. A discretized population balance for continuous systems at steady state. A.I.Ch.E. Journal 36, 106–116.

Hounslow, M.J., Marshall, V.R., Ryall, R.L., 1988. A discretized population balance for nucleation, growth, and aggregation. A.I.Ch.E. Journal 34, 1821–1832.

Hufnagl, H., McIntyre, M., Blass, E., 1991. Dynamic behaviour and simulation of a liquid–liquid extraction column. Chemical Engineering and Technology 14, 301–306.

Hulburt, H., Katz, S., 1964. Some problems in particle technology. A statistical mechanical formulation. Chemical Engineering Science 19, 555–574.

Karlsen, K.H., Lie, K.-A., Natvig, J.R., Nordhaug, H.F., Dahle, H.K., 2001. Operator splitting methods for systems of convective-diffusion equations: nonlinear error mechanisms and correction strategies. Journal of Computational Physics 173, 636–663.

Kentish, S.E., Stevens, G.W., Pratt, H.R.C., 1998. Estimation of coalescence and breakage rate constants within a Kühni column. Industrial and Engineering Chemistry Research 37, 1099–1106.

Klee, A.J., Treybal, R.E., 1956. Rate of rise or fall of liquid drops. A.I.Ch.E. Journal 2, 444–447.

Koren, B., 1993. A robust upwind discretization method for advection, diffusion and source terms. In: Vreugdenhil, C.B., Koren, B. (Eds.), Numerical methods for advection-diffusion problems. Vieweg & Sohn, Braunschweig, pp. 117–138.

Kostoglou, M., Karabelas, A.J., 1994. Evaluation of zero order methods for simulating particle coagulation. Journal of Colloid Interface Science 163, 420–431.

Kostoglou, M., Karabelas, A.J., 1995. Evaluation of numerical methods for simulating an evolving particle size distribution in growth processes. Chemical Engineering Communications 136, 177–199.

Kronberger, T., 1995. Numerische Simulation von Tropfenpopulationen in Extraktionskolonnen. Dissertation, Johannes Kepler Universitat Linz, Linz, 1995.

Kronberger, T., Ortner, A., Zulehner, W., Bart, H.-J., 1994. Numerical determination of drop size distribution in extraction columns. In: Fasano, A. (Ed.), Seventh European Conference on Mathematics in Industry. B.G. Teubner, Stuttgart, pp. 247–254.

Kronberger, T., Ortner, A., Zulehner, W., Bart, H., 1995. Numerical simulation of extraction columns using a drop population model. Computers and Chemical Engineering 19, S639–S644.

Kumar, S., Ramkrishna, D., 1996a. On the solution of population balance equations by discretization—I. A fixed pivot technique. Chemical Engineering Science 51, 1311–1332.

Kumar, S., Ramkrishna, D., 1996b. On the solution of population balance equations by discretization—II. A moving pivot technique. Chemical Engineering Science 51, 1333–1342.

Kumar, S., Ramkrishna, D., 1997. On the solution of population balance equations by discretization—III. Nucleation, growth and aggregation of particles. Chemical Engineering Science 52, 4659–4679.

Kurganov, A., Tadmor, E., 2000. New high-resolution central schemes for nonlinear conservation laws and convective diffusion equations. Journal of Computational Physics 160, 241–282.

Lee, G., Yoon, E.S., Lim, Y.I., Le Lann, J.M., Meyer, X.M., Joulia, X., 2001. Adaptive mesh method for the simulation of crystallization processes including agglomeration and breakage: the potassium sulfate system. Industrial and Engineering Chemistry Research 40, 6228–6235.

Lim, Y.I., Le Lann, J.M., Meyer, X.M., Joulia, X., Lee, G., Yoon, E.S., 2002. On the solution of population balance equations (PBE) with accurate front tracking methods in practical crystallization processes. Chemical Engineering Science 57, 3715–3732.

Liou, J.-J., Srienc, F., Fredrickson, A.G., 1997. Solutions of population balance models based on a successive generations approach. Chemical Engineering Science 52, 1529–1540.

Lister, J.D., Smit, D.J., Hounslow, M.J., 1995. Adjustable discretized population balance for growth and aggregation. A.I.Ch.E. Journal 41, 591–603.

Liu, Y., Cameron, T., 2001. A new wavelet-based method for the solution of the population balance equation. Chemical Engineering Science 56, 5283–5294.

Mahoney, A.W., Ramkrishna, D., 2002. Efficient solution of population balances equations with discontinuities by finite elements. Chemical Engineering Science 57, 1107–1119.

McSwain, C.V., Durbin, L.D., 1966. The backflow-cell model for continuous two-phase nonlinear axial holdup and mixing effect. Separation Science 1, 677–700.

Mignard, D., Amin, L., Ni, X.-D., 2003. Population balance modelling of droplets in an oscillatory baffled reactor-using direct measurements of breakage rates constants. Journal of Chemical Technology and Biotechnology 78, 364–369.

Milot, J.F., Duhamet, J., Gourdon, C., Casamatta, G., 1990. Simulation of a pneumatically pulsed liquid–liquid extraction column. Chemical Engineering Journal 45, 111–122.

Modes, G., 2000. Grundsatzliche Studie zur Populationsdynamik einer Extraktionskolonne auf Basis von Einzeltropfenuntersuchungen. Dissertation, Shaker Verlag.

Modes, G., Bart, H.-J., Rodrigue-Perancho, D., Broder, D., 1999. Simulation of the fluid dynamics of solvent extraction columns from single droplet parameters. Chemical Engineering and Technology 22, 231–236.

Mohanty, S., 2000. Modeling of liquid–liquid extraction column: a review. Reviews in Chemical Engineering 16, 199–248.

Motz, S., Mitrovic, A., Gilles, E.-D., 2002. Comparison of numerical methods for the simulation of dispersed phase systems. Chemical Engineering Science 57, 4329–4344.

Nicmanis, M., Hounslow, M.J., 1998. Finite-element methods for steady-state population balance equations. A.I.Ch.E. Journal 44, 2258–2272.

Qian, Y., Wang, J., 1992. Modelling of mass transfer in extraction columns with drop forward-mixing and coalescence-redispersion. Canadian Journal of Chemical Engineering 70, 88–96.

Ramkrishna, D., 1985. The status of population balances. Reviews in Chemical Engineering 5, 49–95.

Ramkrishna, D., 2000. Population Balances: Theory and Applications to Particulate Systems in Engineering. Academic Press, San Diego.

Ribeiro, L.M., Regueiras, P.F.R., Guimaraes, M.M.L., Madureira, C.M.C., Cruz-Pintu, J.J.C., 1995. The dynamic behavior of liquid–liquid agitated dispersions—I. The hydrodynamics. Computers and Chemical Engineering 19, 333–343.

Ribeiro, L.M., Regueiras, P.F.R., Guimaraes, M.M.L., Madureira, C.M.N., Cruz-Pinto, J.J.C., 1997. The dynamic behavior of liquid–liquid agitated dispersions II. Coupled hydrodynamics and mass transfer. Computers and Chemical Engineering 21, 543–558.

Rice, G.R., Do, D.D., 1995. Applied Mathematics and Modeling for Chemical Engineers. Wiley, New York.

Sastry, K.V.S., Gaschignard, P., 1981. Discretization procedure for the coalescence equation of particulate process. Industrial and Engineering Chemistry Fundamentals 20, 355–361.

Song, M., Steif, A., Weinspach, P.-M., 1997. A very effective method to solve the population balance equation with particle size growth. Computers and Chemical Engineering 52, 3493–3498.

Steiner, L., Bamelli, M., Hartland, S., 1999. Simulation of hydrodynamic performance of stirred extraction column. A.I.Ch.E. Journal 45, 257–267.

Toro, E.F., 1999. Riemann Solvers and Numerical Methods for Fluid Dynamics, 2nd Edition. Springer, Berlin.

Toutain, J., Lann, J.M.L., Gourdon, C., Joulia, X., 1998. Maxwell–Stefan approach coupled drop population model for the dynamic simulation of liquid–liquid extraction pulsed column. Computers and Chemical Engineering 22, S379–S386.

Tsouris, C., Kirou, V.I., Tavlarides, L.L., 1994. Drop size distribution and holdup profiles in a multistage extraction column. A.I.Ch.E. Journal 40, 407–418.

Valentas, K.J., Amundson, A.R., 1966. Breakage and coalescence in dispersed phase systems. Industrial and Engineering Chemistry Fundamentals 5, 533–542.

Vanni, M., 1999. Discretization procedure for the breakage equation. A.I.Ch.E. Journal 45, 916–919.

Vanni, M., 2000. Approximate population balances equations for aggregation-breakage processes. Journal of Colloid Interface Science 221, 143–160.

van Peborgh Gooch, J.R., Hounslow, M.J., 1996. Monte Carlo simulation of size-enlargement mechanics in crystallization. A.I.Ch.E. Journal 42, 1864–1874.

Verkoeijen, D., Pauw, G.A., Meesters, G.M.H., Scarlett, B., 2002. Population balances for particulate processes—a volume approach. Chemical Engineering Science 57, 2287–2303.

Vignes, A., 1965. Hydrodynamique des dispersions. Genie Chimique 93, 129–142.

Weinstein, O., Semiat, R., Lewin, D.R., 1998. Modeling, simulation and control of liquid–liquid extraction columns. Chemical Engineering Science 53, 325–339.

Wesselingh, J.A., Bollen, A.M., 1999. Single particles, bubbles and drops: their velocities and mass transfer coefficients. Transactions of the Institution of Chemical Engineers 77, 89–96.

Wilburn, N.P., 1964. Mathematical determination of concentration profiles in two-phase continuous countercurrent extractors. Industrial and Engineering Chemistry Fundamentals 3, 189–195.

Wulkow, M., Gerstlauer, A., Nieken, U., 2001. Modeling and simulation of crystallization process using parsival. Chemical Engineering Science 56, 2575–2588.

Zamponi, G., Stichlmair, J., Gerstlauer, A., Gilles, E.-D., 1996. Simulation of the transient behaviour of a stirred liquid/liquid extraction column. Computers and Chemical Engineering 20, S963–S968.

Zhang, S.H., Yu, S.C., Zhou, Y.C., Su, Y.F., 1985. A model for liquid–liquid extraction column performance—The influence of drop size distribution on extraction efficiency. Canadian Journal of Chemical Engineering 63, 212–226.

Zhu, F.G., Ni, X.D., Zhou, Y.C., Yu, S.C., Su, Y.F., 1984. A modified rotating disc contactor with wire mesh coalescers. In: Akell, R., King, C.J. (Eds.), New Developments in Liquid–Liquid Extractors: Selected Papers from ISEC '83, Vol. 80. A.I.Ch.E., New York, pp. 115–123.

Zimmermann, A., Joulia, X., Gourdon, C., Gorak, A., 1995. Maxwell–Stefan approach in extractor design. Chemical Engineering Journal 57, 229–236.